

Development of transit and docking control for milliAmpère

Brage Sæther
December 2018



Department of Engineering Cybernetics
Norwegian University of Science and Technology (NTNU)

Abstract

This report reviews a control theory approach to perform autonomous crossings in a trafficked close quarter waterway. The prototype milliAmpère is used as the experimental platform throughout this project. The prototype is intended as a test platform for control algorithms and sensors. Previous work on the prototype has shown that the properties of maneuverability brings unwanted effects for controlling the vessel.

The main concern about the current solution is the heading instability which introduces unwanted effects in the system. This report looks further into this problem, and proposes a possible solution for this issue. The proposed solution is a combination of known control theory algorithms. The control theory algorithms used includes a Dynamic Positioning (DP), Line-of-Sight (LOS) and velocity controller. The main idea is to combine the strengths of the different controllers such that better overall performance is achieved. The theoretical aspects of each controller is discussed before results from a simulated environment is presented. Afterwards, the results from real life experiments conducted over the course of three days are discussed.

Additionally, the report explores the validity of the different control theory approaches for milliAmpère. The unique design and intended usage of milliAmpère introduces a couple of challenges. These challenges are examined and discussed further.

Preface

This project report is part of a 5 year MSc degree in Engineering Cybernetics at the Norwegian University of Science and Technology (NTNU). This report will serve as research and preparatory work for the MSc thesis.

The author finds the field of autonomous vehicles and vessels very interesting. A curiosity towards self governed systems and the adaptability showcased in autonomous systems, were the main motivators for the author to pursue this project. The future prospects within this field are very bright. The opportunity to take part in the research and development and to further contribute in this field, was one of the main sources of motivation throughout the project.

The potential impact of autonomous vessels in urban waterways is huge. This report applies the use of different control algorithms in such an environment. The intended use of milliAmpère is highly specialized, and the design of the vessel is a direct result of this. The design has interesting effects on how the vessel behaves, and subsequently how it should be controlled. This report looks further into these effects and explores different solutions.

Lastly, I would like to thank my academic supervisors Morten Breivik, Egil Eide and Edmund Brekke for all the help during the course of this project. This includes everything from practical issues with milliAmpère, to valuable tips and insights of writing the report. This has been a fun project to work on, and I'm looking forward to continue the work as part of my MSc thesis.

Brage Sæther
18th December 2018
Trondheim, Norway

Table of Contents

Abstract	I
Preface	II
Table of Contents	III
List of Tables	VI
List of Figures	VII
Abbreviations	IX
1 Introduction	3
1.1 Background	3
1.2 Motivation	4
1.3 Project Description	6
1.4 Contributions	6
1.5 Outline	7
2 Theoretical Background	9
2.1 Reference Frames	9
2.1.1 ECEF frame	10
2.1.2 NED frame	10
2.1.3 BODY frame	11
2.2 Vessel Modelling	13
2.2.1 Kinematics	14
2.2.2 Kinetics	15
2.3 Reference Models	16
2.3.1 Pose Reference Model	16
2.3.2 Velocity Reference Model	18
2.4 Control Algorithms	18
2.4.1 PID controller	19
2.4.2 Velocity Controller	19
2.4.3 Dynamic Positioning Controller	21
2.4.4 Line of Sight Controller	21
2.5 Thrust Allocation	24

3	Experimental Platform	27
3.1	Concept	27
3.2	Components	28
3.3	Previous Work	31
4	Control Design	35
4.1	Reference Models	35
4.1.1	Pose reference Model	35
4.1.2	Velocity Reference Model	37
4.2	Control Algorithms	38
4.2.1	Surge Controller	38
4.2.2	Dynamic Positioning Controller	39
4.2.3	Line of Sight Controller	40
4.3	Transition State	41
4.4	Thrust Allocation	41
5	Simulation Results	43
5.1	Crossing tests	43
5.1.1	Simulated Position	44
5.1.2	Simulated velocities	46
5.2	Discussion	47
6	Experimental Results	49
6.1	Bollard Pull Test	50
6.2	Test Area	51
6.3	Experiments the 30th of November 2018	53
6.3.1	Conditions	53
6.3.2	Intentions	53
6.3.3	Execution	53
6.3.4	Reflections	54
6.4	Experiments the 6th of December 2018	54
6.4.1	Conditions	54
6.4.2	Intentions	55
6.4.3	Execution	55
6.4.4	Reflections	55
6.5	Results	56
6.5.1	Initial Crossing Tests	56
6.5.2	Different Thrust Configurations	58
6.5.3	Tuning of Velocity Reference Model and Surge Controller	59
7	Discussion	63
7.1	Time Challenges	63
7.2	Solution	64
8	Conclusions and Future Work	65
8.1	Conclusions	65

8.2 Future Work	66
Bibliography	67
A Media Coverage	69
B SysML Diagrams	71
C GUI	79
D Arduino Shield Specification	81

List of Tables

2.1 Notation for marine vessels	12
---	----

List of Figures

1.1	Concept for autonomous vessels in urban waterways. Image courtesy of Reaktor	4
1.2	Map of the area for the intended use of the autonomous passenger ferry. Image courtesy of Egil Eide	5
2.1	Relationship between different reference frames. Courtesy of (Fossen, 2011)	10
2.2	Relationships between Euler angles. Courtesy of (Fossen, 2011)	12
2.3	The Body fixed (BODY) frame. χ and ψ denotes the course and heading of the vessel, and u and v denotes the surge and sway. Figure courtesy of (Breivik, 2010)	13
2.4	Motion control block scheme. Courtesy of (Fossen, 2011)	16
2.5	Reference model with saturation of \mathbf{a}_d and \mathbf{v}_d . Courtesy of (Fossen, 2011)	17
2.6	LOS guidance principles, Courtesy of (Fossen, 2011)	22
2.7	Actuator Configuration on milliAmpère	24
3.1	Design of milliAmpère. Courtesy of Jon Boye Andresen, Innovation JBA	28
3.2	Thruster configuration on milliAmpère. Courtesy of Jon Boye Andresen, Innovation JBA	29
3.3	Used Components	30
3.4	Concept of 4 corner test for DP controller. Courtesy of (Lyngstadaas, 2018)	32
3.5	Previously performed 4 corner DP test	33
3.6	Response from individual measurements during 4 corner DP test	34
4.1	Position generated by the pose reference model	36
4.2	Velocity generated by the pose reference model	36
4.3	Acceleration generated by the pose reference model	37
4.4	Generated surge velocity reference	38
5.1	Simulation of a canal crossing. Position and virtual docks are shown . . .	44
5.2	Simulation of canal crossing with heading visualization	45
5.3	Cross track error during simulation of crossing	46
5.4	Surge, Sway and Yaw during simulated crossing	47
6.1	Mapping from percentage of thrust capacity to generated thrust force . . .	51
6.2	Test Area for milliAmpère	52

6.3	First crossing test, Pose	56
6.4	First crossing test, Surge, Sway and Yaw	57
6.5	First crossing test, Position and cross track error	57
6.6	Second crossing test, Pose	58
6.7	Second crossing test, Velocities With Velocity Reference Model	59
6.8	Second crossing test, Position and Cross Track Error	59
6.9	Third crossing test, Pose	60
6.10	Third crossing test, Velocities	60
6.11	Third crossing test, Position and Cross Track Error	61
A.1	Brage (left) on board milliAmpère during a demo at Sjøsikkerhetskonferansen in Haugesund. Photo courtesy of Teknisk Ukeblad	69
B.1	Use Case Diagram	71
B.2	Context Diagram	72
B.3	Interface Diagram	72
B.4	Structure Diagram	73
B.5	Sequence Diagram	73
B.6	State Diagram	74
B.7	Class Diagram	75
B.8	Activity Diagram, Mode Change	76
B.9	Activity Diagram, Determine Input	77
C.1	GUI	79

Abbreviations

BLDC Brushless Direct Current. 29, 30

BODY Body fixed. VII, 9, 11–15, 18, 58

COG Center of Gravity. 14, 28, 53

DOF Degree of Freedom. 12–15, 18, 20, 21, 24, 38, 39, 42

DP Dynamic Positioning. I, VII, 19, 21, 31–36, 39–41, 44, 46, 47, 53, 54, 64

ECEF Earth-centered Earth-fixed. 9–11

EOM Equations of Motion. 13

GES Globally Exponentially Stable. 20

GNSS Global Navigation Satellite System. 10, 28, 30, 31, 53

GUI Graphical User Interface. 31, 79

I/O Input/Output. 29

ILOS Integral Line-of-Sight. 23, 40, 41

IMU Inertial Measurement Unit. 28, 30, 31

LOS Line-of-Sight. I, VII, 6, 19, 21–24, 35, 39–41, 44, 46, 47, 55, 56

NED North-East-Down. 9–12, 14, 15, 23

OBC On Board Computer. 29

PCB Printed Circuit Board. 49

PID Proportional–Integral–Derivative. 19, 21, 39, 41, 53, 55

QP Quadratic Programming. 25, 42

RB rigid-body. 15

RTK Real Time Kinematics. 31

SSI Synchronous Serial Interface. 29, 30

Chapter 1

Introduction

This chapter explores the background and motivation for this project. A short introduction to the various areas of interest are given here. Furthermore, the project description and the contributions made by the author are specified.

1.1 Background

During the last decades there has been a drastic increase of automation. Everything from industrial robots on assembly lines, to small automated lawnmowers has been introduced. Lately, autonomous systems able to solve more complex tasks in more complex environments has emerged. Being able to integrate this technology in todays modes of transportation can serve as a great advance in personal transportation.



Figure 1.1: Concept for autonomous vessels in urban waterways. Image courtesy of Reaktor

Today there are more and more cars and buses on the roads, and bigger cities see an increased problem with traffic. By moving some of the personal transportation onto water, the pressure on the roads can be reduced. Other areas can also have great benefits. By providing an easy mode of transportation across waterways, communities and different parts of cities separated by water can easily be tied together. This opens up a whole array of opportunities. Furthermore, the realization of a digitized ferryman will contribute towards the possibility of a seamless interacting transportation system including autonomous cars, buses, trains and marine vessels.

1.2 Motivation

Many places around Norway suffer from the lack of infrastructure to make it easier for people to get across waterways. Many older solutions such as cable ferries or a ferryman have traditionally had such a role. The main idea behind milliAmpère is to provide a cheap, environmentally friendly and non-intrusive solution to this problem. The ability to provide the same logistical service as bridges, will make sure that smaller ports, harbours and canals are kept open and provides the necessary waterways for big and small vessels alike. The canal between Fosenkaia and Ravnkloa in Trondheim is the intended area for the ferry to operate.



Figure 1.2: Map of the area for the intended use of the autonomous passenger ferry. Image courtesy of Egil Eide

This service has in Trondheim historically been carried out by a local ferryman in a rowing boat. The project is currently in phase two and is focused on the continued development of the prototype milliAmpère.

The finished ferry is to serve as an on-demand ferry that passengers can request based on need. The ferry will accommodate the necessary requirements to maintain safe and secure transportation. Its main goal is to provide passengers with easy, fast and reliable transportation option across urban waterways. The full sized vessel will have the capability to transport 12 passengers at any given time, as well as bikes and similar equipment. Providing a scalable solution will make sure the ferry is easily deployed where it's needed. Not only in Norway is this solution desirable, but it can be used all over the world. The development of milliAmpère also brings with it substantial attention given its autonomous nature. A ferry of this kind will also provide Trondheim with a new attraction of a very unique kind.

1.3 Project Description

The main objective is to develop a first version of the control system for automatic transit and docking for milliAmpère. This means investigating different controllers and their possible usage towards the problem at hand. The project description is summarized as follows:

- Literature study for docking on non-stationary dock.
- Design and implement a LOS controller for transit
- Implement the necessary transitions between controllers.
- Continue development of state machine to accommodate complete crossing and easy switching between states
- Interface the new implementations to the existing software architecture
- Implement and test the solution in simulations and full scale

1.4 Contributions

The main contributions are summarized as:

- Design of Arduino shield to replace the unreliable PCB solution for reading absolute encoders
- Designed and implemented a LOS controller for transit
- Designed and implemented a surge controller
- Implemented a multidirectional crossing control system
- Continued development of the state machine and the necessary switching mechanisms
- Maintained and developed a modular design for easy interfacing to other relevant modules
- Performed extensive testing in a simulated environment to ensure proper implementation
- Performed real life successful experiments for the complete system

There was substantial media coverage around milliAmpère during the course of this project. A short list summarizing the coverage about the ferry is found in Appendix A.

1.5 Outline

This report is organized in chapters and sections. Each chapter is naturally divided into the different topics. The different chapters are organized with the use of this structure:

- Chapter 2 introduces the relevant theory
- Chapter 3 describes the experimental platform and its components
- Chapter 4 describes the control design and the different parameters used
- Chapter 5 discusses results obtained from a simulated environment
- Chapter 6 discusses the real life tests that were performed and their respective results
- Chapter 7 and 8 provides the discussions and the conclusions drawn from the project as a whole

Theoretical Background

This chapter elaborates on the theory for implementation of the control algorithms needed to get the desired behaviour. It follows a natural progression by elaborating on the basic theory before delving deeper into other aspects of theory needed for further implementation.

2.1 Reference Frames

When analyzing the motion of the vessel, it is important to differentiate between different reference frames. The different measurements are given in a specific frame, and it is important to transform the measurement to the correct frame before utilizing its measurement in the model. The different frames need to be separated, and the relationship between them established. The frames of interest are the Earth-centered Earth-fixed (ECEF) given in coordinate system $\{e\}$, North-East-Down (NED) given in coordinate system $\{n\}$ and BODY frame given in coordinate system $\{b\}$.

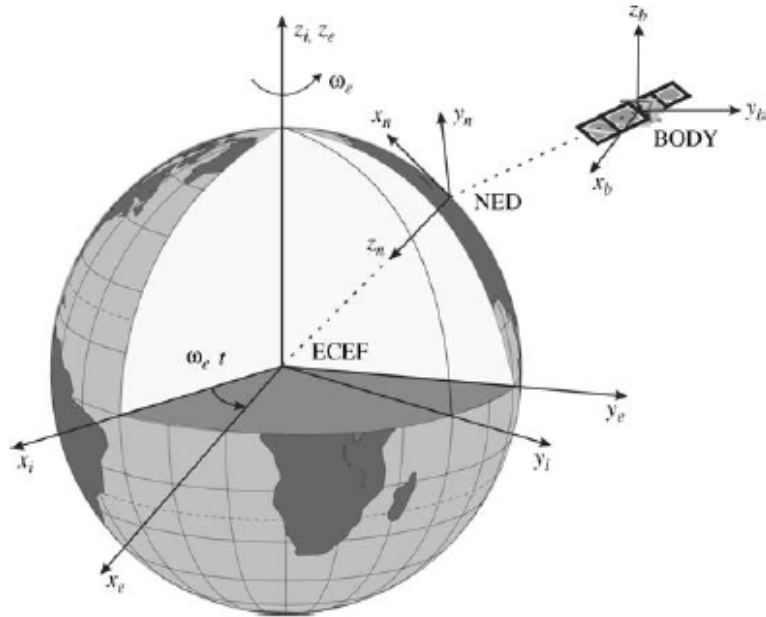


Figure 2.1: Relationship between different reference frames. Courtesy of (Fossen, 2011)

2.1.1 ECEF frame

The ECEF frame is a fixed inertial frame with the origin at the earth's center. Given that it is an inertial frame, Newton's second law of motion applies. The Global Navigation Satellite System (GNSS) gives its coordinates relative to the ECEF frame. The coordinates are given in the standard longitude, latitude and altitude format. By using a transformation, the ECEF frame is transformed into the NED frame.

2.1.2 NED frame

The NED frame is described as a tangent plane to the Earth's surface. The components of the NED frame is given as $[x_n, y_n, z_n]^T$. The coordinates denotes the position in true north, true east and down respectively. The NED frame is a relative frame with origin in Earth's reference ellipsoid defined by (WGS84, 1984). For vessels operating in a small area with small deviations in the longitude and latitude coordinates, the simplification that the NED frame is inertial can be made. This is referred to as the flat Earth approximation. This simplification ensures the validity of Newton's laws of motion in the NED frame.

The transformation between the ECEF frame and the NED frame is described in (Fossen, 2011) as

$$\dot{\mathbf{p}}_{b/e}^e = \mathbf{R}_n^e(\Theta_{\text{en}})\dot{\mathbf{p}}_{b/e}^n = \mathbf{R}_n^e(\Theta_{\text{en}})\mathbf{R}_b^n(\Theta_{\text{nb}})\mathbf{v}_{b/e}^b \quad (2.1)$$

where Θ_{en} is defined as $[l, \mu]^T \in \mathbf{S}^2$ by longitude l and latitude μ . This means that $\mathbf{S}^2 \rightarrow SO(3)$ is given by the rotation matrix $\mathbf{R}_n^e(\Theta_{\text{en}})$. This rotation matrix is given in (Fossen, 2011) and is defined as

$$\mathbf{R}_n^e(\Theta_{\text{en}}) = \mathbf{R}_{z,l}\mathbf{R}_{y,-\mu-\frac{\pi}{2}} \quad (2.2a)$$

$$\mathbf{R}_n^e(\Theta_{\text{en}}) = \begin{bmatrix} -\cos(l)\sin(\mu) & -\sin(l) & -\cos(l)\cos(\mu) \\ -\sin(l)\sin(\mu) & \cos(l) & -\sin(l)\cos(\mu) \\ \cos(\mu) & 0 & -\sin(\mu) \end{bmatrix} \quad (2.2b)$$

2.1.3 BODY frame

The BODY frame is the transformation from the NED frame about the Euler angles given by roll, pitch and yaw. For simplicity, these are from here on out referred to as ϕ , θ and ψ . The rotation matrix about the Euler angles is given in (Fossen, 2011) as

$$\mathbf{R}_b^n(\Theta_{\text{nb}}) = \begin{bmatrix} c\psi c\theta & -s\psi c\theta + c\psi s\theta s\phi & s\psi s\theta + c\psi c\theta s\phi \\ s\psi c\theta & c\psi c\theta + s\phi s\theta s\psi & -c\psi s\theta + s\theta s\psi c\phi \\ -s\theta & c\theta s\phi & c\theta c\phi \end{bmatrix} \quad (2.3)$$

Where $\mathbf{R}_b^n(\Theta_{\text{nb}})$ denotes the rotation $\mathbf{R}_{z,\psi}\mathbf{R}_{y,\theta}\mathbf{R}_{x,\phi}$, $c = \cos$ and $s = \sin$. These angles represent the angular position of a vessel. A visualization of their derivatives, $[\dot{\phi}, \dot{\theta}, \dot{\psi}] = [p, q, r]$, is shown in Figure 2.2.

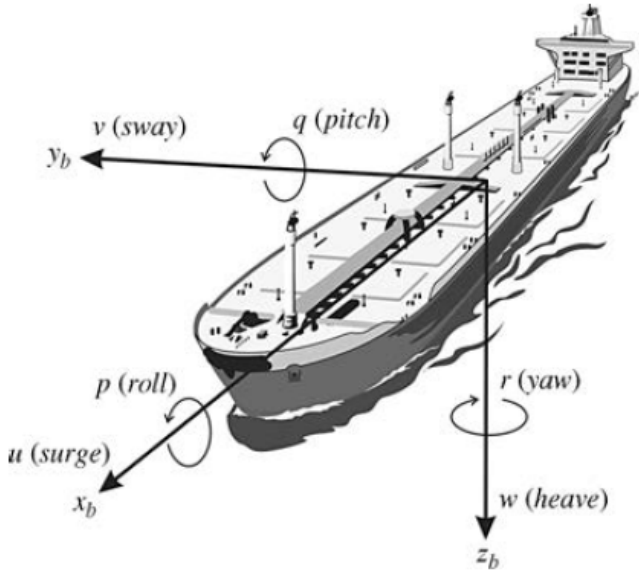


Figure 2.2: Relationships between Euler angles. Courtesy of (Fossen, 2011)

For a marine vessel, the ϕ and θ angles are negligible. The transformation between NED and BODY frame is reduced to the rotation around the z axis with the angle ψ . This rotation is given by

$$\mathbf{R}_b^n(\psi) = \begin{bmatrix} \cos(\psi) & -\sin(\psi) & 0 \\ \sin(\psi) & \cos(\psi) & 0 \\ 0 & 0 & 1 \end{bmatrix} \quad (2.4)$$

This rotation refers to the BODY frame. In the BODY frame, the six motion components are described using the notations defined in (SNAME, 1950). The motions and rotations are given by Table 2.1.

Degree of Freedom (DOF)		Forces and moments	Linear and angular velocities	Positions and Euler angles
1	motions in the x direction (surge)	X	u	x
2	motions in the y direction (sway)	Y	v	y
3	motions in the z direction (heave)	Z	w	z
4	rotation about the x axis (roll, heel)	K	p	ϕ
5	rotation about the y axis (pitch, trim)	N	q	θ
6	rotation about the z axis (yaw)	M	r	ψ

Table 2.1: Motion and rotation notation for marine vessels defined in (SNAME, 1950)

The BODY frame has notations for different velocities and different rotations. The various relationships in BODY frame are shown in Figure 2.3.

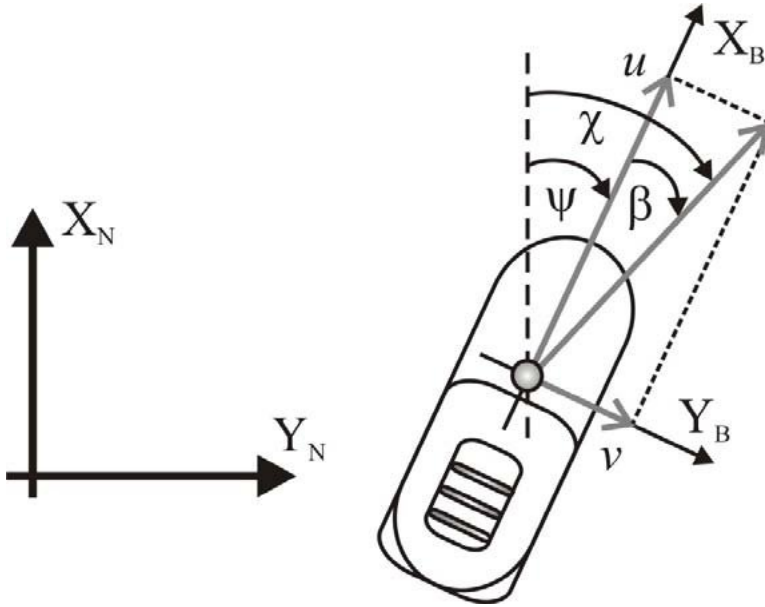


Figure 2.3: The BODY frame. χ and ψ denotes the course and heading of the vessel, and u and v denotes the surge and sway. Figure courtesy of (Breivik, 2010)

2.2 Vessel Modelling

The vessel is modelled using kinematics and kinetics. The resulting model used going forward is a 3 DOF system model. This 3 DOF model is obtained by neglecting the non-relevant states in the full 6 DOF model.

When describing the Equations of Motion (EOM) for a marine vessel, proper vector notation is needed. In (Fossen, 2011), the 6 DOF rigid-body EOM according to the (SNAME, 1950) notation, is written in component form as

$\mathbf{f}_b^b = [X, Y, Z]^T$	– force through o_b expressed in $\{b\}$
$\mathbf{m}_b^b = [K, M, N]^T$	– moment about o_b expressed in $\{b\}$
$\mathbf{v}_{b/n}^b = [u, v, w]^T$	– linear velocity of o_b relative o_n expressed in $\{b\}$
$\mathbf{w}_{b/n}^b = [p, q, r]^T$	– angular velocity of $\{b\}$ relative to $\{n\}$ expressed in $\{b\}$
$\mathbf{r}_g^b = [x_g, y_g, z_g]^T$	– vector from o_b to Center of Gravity (COG) expressed in $\{b\}$
$\mathbf{p}_{n/b}^n = [N, E, D]^T$	– distance from $\{n\}$ to $\{b\}$ expressed in $\{n\}$
$\Theta_{nb} = [\phi, \theta, \psi]^T$	– Euler angles between $\{n\}$ and $\{b\}$

2.2.1 Kinematics

A 6 DOF kinematic equation for a vessel in motion is expressed in (Fossen, 2011) as

$$\dot{\boldsymbol{\eta}} = \mathbf{J}_\Theta(\boldsymbol{\eta})\boldsymbol{\nu} \quad (2.5a)$$

$$\begin{bmatrix} \dot{\mathbf{p}}_{b/n}^n \\ \dot{\Theta}_{nb} \end{bmatrix} = \begin{bmatrix} \mathbf{R}_b^n(\Theta_{nb}) & \mathbf{0}_{3 \times 3} \\ \mathbf{0}_{3 \times 3} & \mathbf{T}_\Theta(\Theta_{nb}) \end{bmatrix} \begin{bmatrix} \mathbf{v}_{b/n}^b \\ \boldsymbol{\omega}_{b/n}^b \end{bmatrix} \quad (2.5b)$$

where $\mathbf{p}_{b/n}^n = [x, y, z]^T$ and $\Theta_{nb} = [\phi, \theta, \psi]^T$ are the positions and Euler angles respectively, and \mathbf{J}_Θ is the transformation matrix between the BODY and NED frame.

As discussed in Section 2.1.3, for a marine surface vessel ϕ, θ and z are negligible. The surface vessel is therefore restricted to horizontal motion and rotation around the z -axis. These motions are referred to as surge, sway and yaw. The simplification of neglecting heave, roll and pitch is made. As a result, the state space reduces to a 3 DOF system. The transformation matrix $\mathbf{J}_\Theta(\boldsymbol{\eta})$ reduces to the rotation around the z -axis. This means that the transformation matrix reduces to (2.4) and is given by

$$\mathbf{J}_\Theta(\boldsymbol{\eta}) = \mathbf{R}(\psi) = \begin{bmatrix} \cos(\psi) & -\sin(\psi) & 0 \\ \sin(\psi) & \cos(\psi) & 0 \\ 0 & 0 & 1 \end{bmatrix} \quad (2.6)$$

The kinematic equation for the 3 DOF system becomes

$$\dot{\boldsymbol{\eta}} = \mathbf{R}(\psi)\boldsymbol{\nu} \quad (2.7)$$

where the state space vectors are reduced to $\boldsymbol{\eta} = [x, y, \psi]^T$ and $\boldsymbol{\nu} = [u, v, r]^T$.

2.2.2 Kinetics

A 6 DOF system can be described with the rigid-body (RB) kinetics described in (Fossen, 2011) as

$$M\dot{\boldsymbol{\nu}} + \mathbf{C}(\boldsymbol{\nu})\boldsymbol{\nu} + \mathbf{D}(\boldsymbol{\nu})\boldsymbol{\nu} + \mathbf{g}(\boldsymbol{\eta}) + \mathbf{g}_0 = \boldsymbol{\tau} + \boldsymbol{\tau}_{wind} + \boldsymbol{\tau}_{wave} \quad (2.8)$$

where

$$\mathbf{M} = \underbrace{\begin{bmatrix} m\mathbf{I}_{3 \times 3} & m\mathbf{S}(\mathbf{r}_g^b) \\ m\mathbf{S}(\mathbf{r}_g^b) & \mathbf{I}_b \end{bmatrix}}_{\mathbf{M}_{RB}} + \mathbf{M}_A \quad (2.9a)$$

$$\mathbf{C} = \underbrace{\begin{bmatrix} m\mathbf{I}_{3 \times 3} & m\mathbf{S}(\mathbf{r}_g^b) \\ m\mathbf{S}(\mathbf{r}_g^b) & \mathbf{I}_b \end{bmatrix}}_{\mathbf{C}_{RB}(\boldsymbol{\nu})} + \mathbf{C}_A(\boldsymbol{\nu}) \quad (2.9b)$$

$$\mathbf{D} = \mathbf{D}_v(\boldsymbol{\nu}) + \mathbf{D}_n(\boldsymbol{\nu}) \quad (2.9c)$$

where \mathbf{M} , $\mathbf{C}(\boldsymbol{\nu})$ and $\mathbf{D}(\boldsymbol{\nu})$ are the inertia, coriolis and damping matrices respectively, and $\mathbf{g}(\boldsymbol{\eta})$ denote the generalized gravitaional and buoyancy forces. Static restoring forces and moments are collected in the term \mathbf{g}_0 . The relevant motions are described by surge, sway and yaw. The states of interest are the North-East-Heading positions given by $\boldsymbol{\eta} = [N, E, \psi]^T$ in the NED frame, and velocities surge, sway and yaw described by $\boldsymbol{\nu} = [u, v, r]^T$ in the BODY frame.

The complete kinematic and kinetic model for a marine vessel in 3 DOF is then described as

$$\dot{\boldsymbol{\eta}} = \mathbf{J}_{\Theta}(\boldsymbol{\eta})\boldsymbol{\nu} \quad (2.10a)$$

$$\mathbf{M}\dot{\boldsymbol{\nu}} + \mathbf{C}_{RB}(\boldsymbol{\nu})\boldsymbol{\nu} + \mathbf{N}(\boldsymbol{\nu}_r)\boldsymbol{\nu}_r = \boldsymbol{\tau} + \boldsymbol{\tau}_{wind} + \boldsymbol{\tau}_{wave} \quad (2.10b)$$

where $\mathbf{N}(\boldsymbol{\nu}_r)\boldsymbol{\nu}_r = \mathbf{C}_A(\boldsymbol{\nu}_r)\boldsymbol{\nu}_r + \mathbf{D}(\boldsymbol{\nu}_r)\boldsymbol{\nu}_r$ and $\boldsymbol{\nu}_r = \boldsymbol{\nu}^b - \boldsymbol{\nu}_c^b$. Here $\boldsymbol{\nu}_c^b$ denotes the current speed in BODY frame. The relations between the vessel and the motion control system is shown in the block scheme in Figure 2.4.

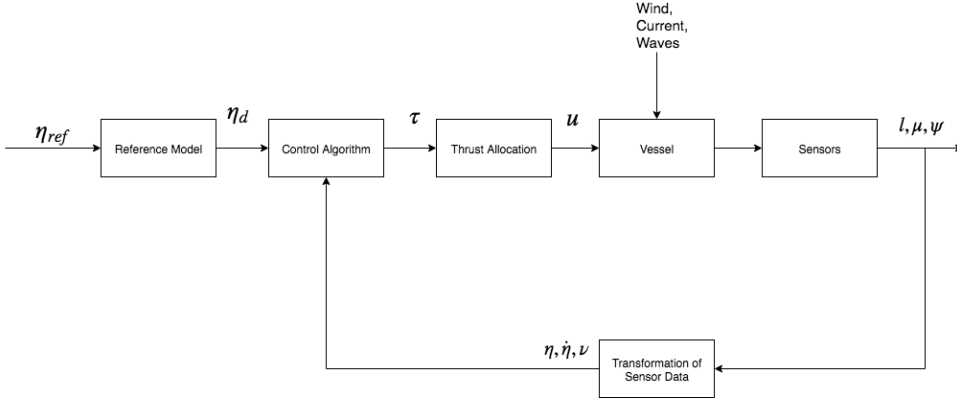


Figure 2.4: Motion control block scheme. Courtesy of (Fossen, 2011)

The other blocks in the block scheme are discussed in more detail in sections 2.3-2.5.

2.3 Reference Models

Reference models are used to generate smooth trajectories based on a desired output. These generated trajectories are applied as input in the various controllers. There are two reference models used in this system. These are a pose reference model and a velocity reference model. The relationship between the reference models and the rest of the motion control system is visualized in the block scheme in Figure 2.4.

2.3.1 Pose Reference Model

By utilizing higher order derivatives of the pose, it can be guaranteed generation of smooth attainable and feasible reference trajectories for the system. It is important to have all the constraints for the relevant controller incorporated in this reference model. In this case, the important constraints are the max acceleration and max velocity.

The pose reference model is given in (Fossen, 2011) in vectorial form as

$$\ddot{\eta}_d + (2\Delta_p + I)\Omega_p\dot{\eta}_d + (2\Delta_p + I)\Omega_p^2\eta_d + \Omega_p^3\eta_d = \Omega_p^3r^n \quad (2.11)$$

The state-space representation for this equation is

$$A_d = \begin{bmatrix} \mathbf{0} & \mathbf{I} & \mathbf{0} \\ \mathbf{0} & \mathbf{0} & \mathbf{I} \\ -\Omega_p^3 & -(2\Delta_p + I)\Omega_p^2 & -(2\Delta_p + I)\Omega_p \end{bmatrix}, \quad B_d = \begin{bmatrix} \mathbf{0} \\ \mathbf{0} \\ \Omega_p^3 \end{bmatrix} \quad (2.12)$$

where $\mathbf{\Omega}_p > 0$ and $\mathbf{\Delta}_p > 0$ in (2.11) and (2.12) are diagonal matrices containing the damping ratios ζ_{p_m} and the natural frequencies $\omega_{n_{p_m}}$, and \mathbf{I} is the identity matrix. The damping ratios and natural frequencies are given by

$$\mathbf{\Delta}_p = \text{diag} \{ \zeta_{p_1}, \zeta_{p_2}, \dots, \zeta_{p_m} \} \quad (2.13a)$$

$$\mathbf{\Omega}_p = \text{diag} \{ \omega_{n_{p_1}}, \omega_{n_{p_2}}, \dots, \omega_{n_{p_m}} \} \quad (2.13b)$$

To calculate the desired pose trajectory, (2.11) is used. Based on the desired jerk, $\ddot{\eta}$, the desired values for any given step k , is calculated with the use of Euler integration.

$$\eta_d(k+1) = \eta_d(k) + \nu_d(k+1)dt \quad (2.14a)$$

$$\nu_d(k+1) = \nu_d(k) + \mathbf{a}_d(k+1)dt \quad (2.14b)$$

$$\mathbf{a}_d(k+1) = \mathbf{a}_d(k) + \ddot{\eta}_d(k+1)dt \quad (2.14c)$$

$$\ddot{\eta}_d(k+1) = \mathbf{\Omega}_p^3 \mathbf{r}^n - (2\mathbf{\Delta}_p + \mathbf{I})\mathbf{\Omega}_p \mathbf{a}_d(k) - (2\mathbf{\Delta}_p + \mathbf{I})\mathbf{\Omega}_p^2 \nu_d(k) - \mathbf{\Omega}_p^3 \eta_d(k) \quad (2.14d)$$

While integrating to find the correct pose reference, it is important to enforce any constraints the system has. The saturation function is introduced for this purpose. The saturation function is given by (2.15) below.

$$\text{sat}(x) = \begin{cases} \text{sgn}(x)x_{max} & \text{if } |x| \geq x_{max} \\ x & \text{else} \end{cases} \quad (2.15)$$

By using the saturation function, a realistic reference state η_d is obtained. More details about the different controllers will follow in section 2.4. The pose reference model can be visualized with the block scheme showed in Figure 2.5.

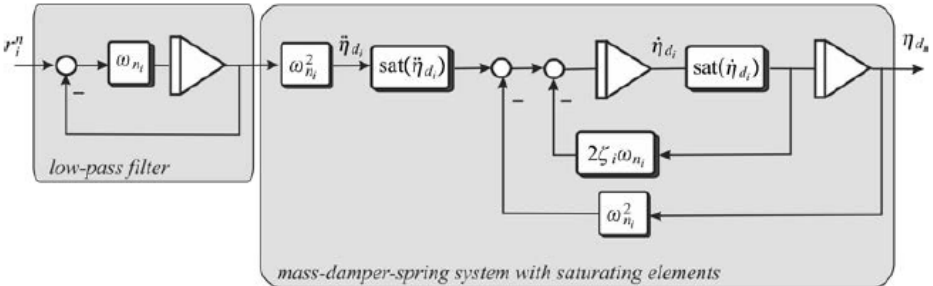


Figure 2.5: Reference model with saturation of \mathbf{a}_d and ν_d . Courtesy of (Fossen, 2011)

2.3.2 Velocity Reference Model

For a velocity controller it is advantageous to use a reference model to generate a feasible continuous desired input to the controller. This is to avoid any unintentional bumps as a result of a step response. Such a reference model is of order two such that the generated velocity reference is a smooth signal. A velocity reference model for this purpose is defined in (Fossen, 2011) as

$$\ddot{\nu}_d + 2\Delta_v\Omega_v\dot{\nu}_d + \Omega_v^2\nu_d = \Omega_v^2r^b \quad (2.16)$$

ν_d is the desired velocity, $\dot{\nu}_d$ is the desired acceleration, $\ddot{\nu}_d$ is calculated as the desired jerk, and r^b is the input for the reference model. r^b represents the wanted velocity in 3 DOF for the system expressed in the BODY frame. The same model can be expressed in matrix form as

$$A_d = \begin{bmatrix} \mathbf{0} & I \\ -\Omega_v^2 & -2\Delta_v\Omega_v \end{bmatrix}, \quad B_d = \begin{bmatrix} \mathbf{0} \\ \Omega_v^2 \end{bmatrix} \quad (2.17)$$

The reference model generates a feasible input for the velocity controller based on the model parameters. $\Omega_v > 0$ and $\Delta_v > 0$ are constant matrices defined by

$$\Delta_v = \text{diag} \{ \zeta_{v_1}, \zeta_{v_2}, \dots, \zeta_{v_m} \} \quad (2.18a)$$

$$\Omega_v = \text{diag} \{ \omega_{n_{v_1}}, \omega_{n_{v_2}}, \dots, \omega_{n_{v_m}} \} \quad (2.18b)$$

These parameters define the behaviour of the vessel and subsequently the reference model. The desired jerk, $\ddot{\nu}_d$, is calculated from (2.16). ν_d is found by Euler integration similar to (2.14).

2.4 Control Algorithms

In this system there are various controllers that serve different purposes. This section establishes these controllers, and provides the theory behind them. The relationship between the controllers and the rest of the motion control system is shown in Figure 2.4.

2.4.1 PID controller

The controllers in this system are based on one basic controller. This controller forms the basis of other control algorithms that control the system as a whole. This controller is called a Proportional–Integral–Derivative (PID) controller. A PID controller can have certain additives such as integrator anti windup and negation of derivative kick.

The PID controller is used to minimize an error given between the actual state and the reference state. The PID controller utilizes the error between these states and calculates a desired output. The continuous time PID controller is given by

$$\tau_{pid} = \mathbf{K}_p e + \mathbf{K}_i \int_0^t e(\tau) d\tau + \mathbf{K}_d \dot{e} \quad (2.19a)$$

$$e = \mathbf{x}_d - \mathbf{x} \quad (2.19b)$$

where e is the error state, \dot{e} is the differentiated error state and $\mathbf{K}_p > 0$, $\mathbf{K}_i > 0$ and $\mathbf{K}_d > 0$ are the gain matrices in the controller. The controller used in this system is the discrete PID controller. The discrete version of the PID controller is given by

$$\tau_{pid} = \mathbf{K}_p e(k) + \mathbf{K}_i \sum_{k=0}^k e(k) + \frac{1}{h} \mathbf{K}_d (e(k) - e(k-1)) \quad (2.20)$$

where $h > 0$ is the timestep and $e(k)$ is the error state in the current iteration. This controller is the basis for every controller in the system and is applied in the DP controller, the LOS controller, the velocity controller and for the controller that sets the correct azimuth angle.

Integrator Anti Windup

For any control algorithm that uses the traditional control algorithm discussed in Section 2.4.1, certain things need to be considered. In this case, the one of interest is the integrator anti windup. Integrator anti windup is a precautionary step that is taken when the control algorithm wants to output the maximum or minimum allowed output over time. This can result in the error growing over time when the system has no way of acting on it. This accumulated error can propagate to a scenario where the integral effect is not desired. This could result in undesirable behaviour, or in worst case instability.

2.4.2 Velocity Controller

To utilize the velocity reference model discussed in Section 2.3.2, there is need for a velocity controller. This controller uses the reference that the velocity reference model outputs to decide the correct input for the actuators. The main goal being that the vessel follows

the desired velocity. The velocity controller is based on a nonlinear marine craft model on the form

$$M\dot{\boldsymbol{\nu}} + \mathbf{C}(\boldsymbol{\nu})\boldsymbol{\nu} + \mathbf{D}(\boldsymbol{\nu})\boldsymbol{\nu} + \mathbf{g}(\boldsymbol{\eta}) = \boldsymbol{\tau} \quad (2.21)$$

To be able to get the desired output $\boldsymbol{\tau}$ such that the vessel follows the desired velocity, model based feed forward is utilized to cancel out the non linear behaviour. By using feedback linearization, the desired output $\boldsymbol{\tau}$ is expressed as

$$\boldsymbol{\tau} = M\mathbf{a}^b + \mathbf{C}(\boldsymbol{\nu})\boldsymbol{\nu} + \mathbf{D}(\boldsymbol{\nu})\boldsymbol{\nu} + \mathbf{g}(\boldsymbol{\eta}) \quad (2.22)$$

where \mathbf{a}^b is the commanded acceleration. The commanded acceleration is defined in (Fossen, 2011) by

$$\mathbf{a}^b = \dot{\boldsymbol{\nu}}_d - \mathbf{K}_p\tilde{\boldsymbol{\nu}} - \mathbf{K}_i \int_0^t \tilde{\boldsymbol{\nu}}(\tau)d\tau \quad (2.23a)$$

$$\tilde{\boldsymbol{\nu}} = \boldsymbol{\nu} - \boldsymbol{\nu}_d \quad (2.23b)$$

where $\dot{\boldsymbol{\nu}}_d$ is the desired acceleration provided by the velocity reference model discussed in section 2.3.2 and $\mathbf{K}_p > 0$ and $\mathbf{K}_i > 0$ are the gain matrices. This means that the final desired output $\boldsymbol{\tau}$ takes the form

$$\boldsymbol{\tau} = M(\dot{\boldsymbol{\nu}}_d - \mathbf{K}_p\tilde{\boldsymbol{\nu}} - \mathbf{K}_i \int_0^t \tilde{\boldsymbol{\nu}}(\tau)d\tau) + \mathbf{C}(\boldsymbol{\nu})\boldsymbol{\nu} + \mathbf{D}(\boldsymbol{\nu})\boldsymbol{\nu} + \mathbf{g}(\boldsymbol{\eta}) \quad (2.24)$$

By choosing $\boldsymbol{\tau}$ in this manner, the error dynamics become

$$\dot{\tilde{\boldsymbol{\nu}}} + \mathbf{K}_p\tilde{\boldsymbol{\nu}} + \mathbf{K}_i \int_0^t \tilde{\boldsymbol{\nu}}(\tau)d\tau = 0 \quad (2.25)$$

According to (Fossen, 2011), this controller will be Globally Exponentially Stable (GES) if the gains are chosen as

$$\mathbf{K}_p = \text{diag}(2\lambda_1, 2\lambda_2, \dots, 2\lambda_n) \quad (2.26)$$

$$\mathbf{K}_i = \text{diag}(\lambda_1^2, \lambda_2^2, \dots, \lambda_n^2) \quad (2.27)$$

where $\boldsymbol{\lambda} = [\lambda_1, \lambda_2, \dots, \lambda_n]^T$ represent the eigenvalues of the closed loop system given by (2.25). $\boldsymbol{\tau}$ is the 3 DOF force vector that will ensure that the vessel velocity converges to the desired specified velocity given by $\boldsymbol{\nu}_d$.

2.4.3 Dynamic Positioning Controller

A dynamic positioning controller is a fully actuated control system and its intended use is for low-speed maneuvering and station keeping. This is achieved through driving the state of the system to the given reference, or equivalently $e(t) \rightarrow 0$. $e(t)$ is given in by

$$e(t) = \mathbf{R}^T(\psi)(\boldsymbol{\eta}(t) - \boldsymbol{\eta}_d(t)) = \mathbf{R}^T(\psi) \begin{bmatrix} N(t) - N_d(t) \\ E(t) - E_d(t) \\ \psi(t) - \psi_d(t) \end{bmatrix} \quad (2.28)$$

To establish a control plant to control our system, the low-frequency control plant defined in (Sørensen, 2018) is employed. This is defined as

$$\dot{\boldsymbol{\eta}} = \mathbf{R}(\psi)\boldsymbol{\nu} \quad (2.29a)$$

$$\mathbf{M}\dot{\boldsymbol{\nu}} + \mathbf{D}(\boldsymbol{\nu}) + \mathbf{R}^T(\psi)\mathbf{G}\boldsymbol{\eta} = \boldsymbol{\tau} + \mathbf{R}^T(\psi)\mathbf{b} \quad (2.29b)$$

where $\boldsymbol{\nu} = [u, v, r]^T$, $\boldsymbol{\eta} = [x, y, \psi]^T$, $\mathbf{b} \in \mathbb{R}^3$ is the bias vector and $\boldsymbol{\tau} = [F_x, F_y, \tau_\psi]$ is the force vector.

The controller should be designed to correctly set the desired $\boldsymbol{\tau}$. $\boldsymbol{\tau}$ can be written as

$$\boldsymbol{\tau} = \boldsymbol{\tau}_{pid} + \boldsymbol{\tau}_{ref_{FF}} + \boldsymbol{\tau}_{wind} + \boldsymbol{\tau}_{current} \quad (2.30)$$

where $\boldsymbol{\tau}_{pid}$ is a conventional PID controller in 3 DOF, $\boldsymbol{\tau}_{ref_{FF}}$ is the reference feed forward, and $\boldsymbol{\tau}_{wind}$ and $\boldsymbol{\tau}_{current}$ are the external disturbances. $\boldsymbol{\tau}_{pid}$ is written as

$$\boldsymbol{\tau}_{pid} = -\mathbf{K}\mathbf{e} = -\mathbf{K}_p\mathbf{e} - \mathbf{K}_i \int_0^t \mathbf{e}d\tau - \mathbf{K}_d\dot{\mathbf{e}} \quad (2.31a)$$

$$\mathbf{e} = \mathbf{R}^T(\psi)(\boldsymbol{\eta} - \boldsymbol{\eta}_d) \quad (2.31b)$$

where \mathbf{e} is the error state, $\dot{\mathbf{e}}$ is the differentiated error state, $\boldsymbol{\eta} = [x, y, \psi]^T$, $\boldsymbol{\eta}_d = [x_d, y_d, \psi_d]^T$ and $\mathbf{K}_p > 0$, $\mathbf{K}_i > 0$ and $\mathbf{K}_d > 0$ are the gain matrices in $\mathbb{R}^{3 \times 3}$. The DP controller serves a vital part of the system when it is in use. The DP controller will be in the block noted as Control Algorithm in Figure 2.4.

2.4.4 Line of Sight Controller

A LOS controller is a controller made to follow a time independent path between two given geographical points. This path is predefined by the use of two waypoints. A waypoint is a pose defined by the vector $\boldsymbol{\eta}_{ref} = [N_{ref}, E_{ref}, \psi_{ref}]^T$. The main control objective is to minimize the cross-track error between the vessel and the path defined between the two waypoints. The cross track error is denoted as e in Figure 2.6.

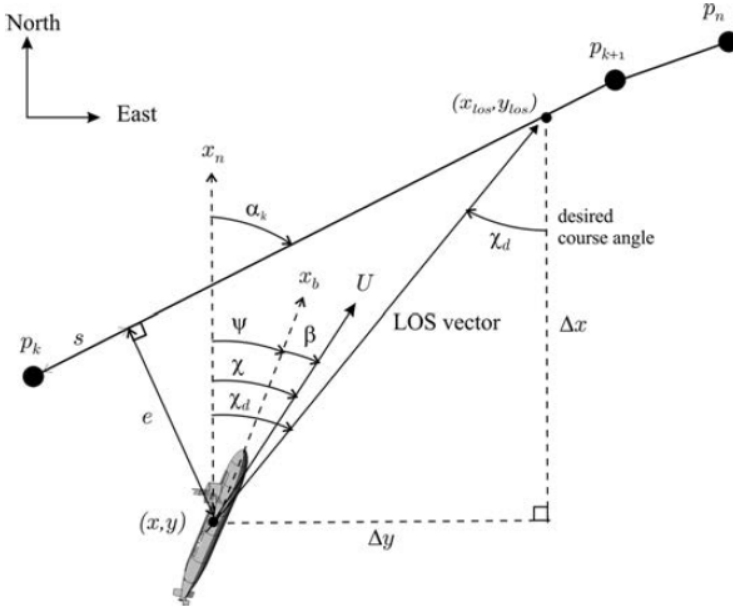


Figure 2.6: LOS guidance principles, Courtesy of (Fossen, 2011)

Line of Sight steering law

A LOS controller depends on certain measurements. The measurements are used to obtain the parameters specified in (Fossen, 2011) by

$$U(t) = |\mathbf{v}(t)| = \sqrt{\dot{x}(t)^2 + \dot{y}(t)^2} \geq 0 \quad (2.32a)$$

$$\chi(t) = \text{atan2}(\dot{y}(t), \dot{x}(t)) \quad (2.32b)$$

$$\alpha_k = \text{atan2}(y_{k+1} - y_k, x_{k+1} - x_k) \quad (2.32c)$$

$$\boldsymbol{\varepsilon}(t) = \mathbf{R}_p(\alpha_k)^T (\mathbf{p}^n(t) - \mathbf{p}_k^n) \quad (2.32d)$$

where $U(t)$ is the given speed, χ is the course angle and α_k is the angle of the desired straight line path. The rotation matrix $\mathbf{R}_p(\alpha_k)$ is given as

$$\mathbf{R}_p(\alpha_k) = \begin{bmatrix} \cos(\alpha_k) & -\sin(\alpha_k) \\ \sin(\alpha_k) & \cos(\alpha_k) \end{bmatrix} \in SO(2) \quad (2.33)$$

The error term is $\boldsymbol{\varepsilon}(t) = [s(t), e(t)]^T$ where $s(t)$ is the along-track distance tangential to the path, and $e(t)$ is the cross-track error perpendicular to the intended straight line path.

Line of sight steering can be performed either as enclosure-based steering or as lookahead-based steering. The controller used here is based on lookahead steering. The desired heading is based on the desired course. The desired course angle is denoted as $\chi_d(e)$, where e is the cross-track error described before. χ_p is the path-tangential angle with regards to the NED frame, and $\chi_r(e)$ is the relative angle for the velocity-path. These components are defined as follows

$$\chi_d(e) = \chi_p + \chi_r(e) \quad (2.34a)$$

$$\chi_p = \alpha_k \quad (2.34b)$$

$$\chi_r(e) = \arctan\left(\frac{-e(t)}{\Delta}\right) \quad (2.34c)$$

Here $\Delta > 0$ denotes the lookahead distance for the controller given in metres. If the lookahead distance is chosen small, the controller becomes more aggressive.

The last step is to use the desired course angle to calculate the desired heading angle. The correlation between the heading angle and the course can be visualized in Figure 2.6. This correlation gives the LOS steering law given by

$$\psi_d = \chi_d - \beta \quad (2.35)$$

Where ψ_d is the desired heading, χ_d is the desired course and β is the sideslip. The sideslip describes how fast the ship moves laterally compared to its speed tangential to the vessels course. The sideslip is defined by the relationship

$$\beta = \arcsin\left(\frac{v}{U}\right) \quad (2.36)$$

Integral line of sight steering law

In (Caharija et al., 2012), there was developed an improved method for Integral Line-of-Sight (ILOS) control. This was based on the ILOS controller proposed by (Børhaug, 2008). The proposed guidance law was designed to drive the cross track error to zero when the vessel is subjected to a slowly varying unknown disturbance. The ILOS steering law is given by

$$\psi_{ILOS} = -\arctan\left(\frac{e + \sigma e_{int}}{\Delta}\right) \quad (2.37a)$$

$$\dot{e}_{int} = \frac{\Delta e}{\sqrt{\Delta^2 + (e + \sigma e_{int})^2}} \quad (2.37b)$$

where e is the cross track error, $\Delta > 0$ is the lookahead distance, $\sigma > 0$ is a tune-able integral gain and \dot{e}_{int} is the integral state of the cross track error. By introducing this integral error state, the error input will build up when the the external disturbances pushes the vessel away from the desired path. By the design of the control law, (2.37) will reduce to (2.34) when there is no disturbance.

The LOS controller will be in place of the control algorithm block in Figure 2.4. The LOS controller only uses the attitude reference signal from the reference model to generate a trajectory for ψ_d while using η_{ref} to navigate to the desired position.

2.5 Thrust Allocation

The vessel milliAmpère operates in 3 DOF. When the vessel is operated by a controller that outputs a desired 3 DOF force, it is necessary to map the desired generalized forces, $\tau = [F_x, F_y, \tau_\psi]^T$, to feasible actuator inputs. For a block scheme showing the relationship between the control allocation and the rest of the motion control system, see Figure 2.4.

For milliAmpère, the actuators in question are two azimuth thrusters. A further visualization of the actuator configuration is shown in Figure (2.7).

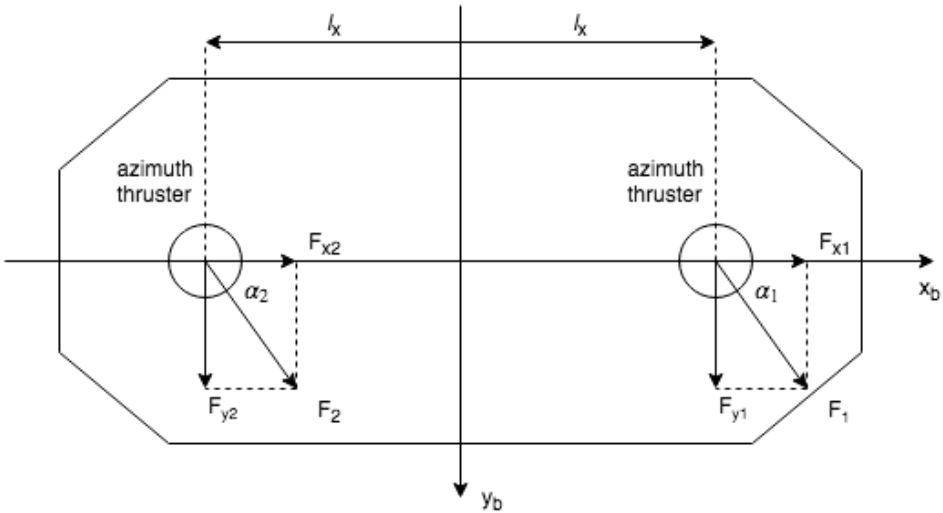


Figure 2.7: Actuator Configuration on milliAmpère

For the current actuator setup, the relationship between the output force τ and the actuator inputs u is described by

$$\boldsymbol{\tau} = \mathbf{T}(\boldsymbol{\alpha})\mathbf{f} = \mathbf{T}(\boldsymbol{\alpha})\mathbf{K}\mathbf{u} \quad (2.38)$$

where $\mathbf{T}(\boldsymbol{\alpha})\mathbf{K}\mathbf{u}$ is called the thrust configuration matrix. \mathbf{K} is the relationship between the thruster input \mathbf{u} and thruster force output \mathbf{f} . $\mathbf{T}(\boldsymbol{\alpha})\mathbf{K}\mathbf{u}$ describes the relationship between the angles and thrust of the azimuth thrusters and the resulting force and torque. For this vessel the thrust configuration matrix becomes

$$\boldsymbol{\tau} = \begin{bmatrix} \cos(\alpha_1) & \cos(\alpha_2) \\ \sin(\alpha_1) & \sin(\alpha_2) \\ l_x \sin(\alpha_1) & -l_x \sin(\alpha_2) \end{bmatrix} \begin{bmatrix} K & 0 \\ 0 & K \end{bmatrix} \begin{bmatrix} u_1 \\ u_2 \end{bmatrix} \quad (2.39)$$

The explicit solution to this problem can be expressed by the pseudoinverse. By use of the pseudoinverse, the actuator input vector \mathbf{u} is defined in (Fossen, 2011) as

$$\mathbf{u} = \mathbf{K}^{-1}\mathbf{T}_w^\dagger(\boldsymbol{\alpha})\boldsymbol{\tau} \quad (2.40a)$$

$$\mathbf{T}_w^\dagger = \mathbf{W}^{-1}\mathbf{T}^T(\boldsymbol{\alpha})[\mathbf{T}(\boldsymbol{\alpha})\mathbf{W}^{-1}\mathbf{T}^T(\boldsymbol{\alpha})]^{-1} \quad (2.40b)$$

where \mathbf{T}_w^\dagger is the pseudoinverse and \mathbf{W} is the weighing matrix. By using the pseudoinverse, the problem is solved as an unconstrained control allocation problem. This is not desirable, and it is necessary to take the different constraints of the system into account.

The process of finding the constrained feasible input \mathbf{u} from the desired output force $\boldsymbol{\tau}$, is described as a model-based optimization problem. The optimization problem is a constrained optimization problem as the thrusters have a constrained thruster force, and the rotation of the thrusters have a constrained rotation speed. For any rotational thruster, there are numerous possible solutions to a desired output force. This optimization problem then becomes non-convex, which is harder to solve. This optimization problem is formulated as a Quadratic Programming (QP) problem. A simple QP problem is defined as

$$J = \min_{\mathbf{f}, \mathbf{s}} \left\{ \sum_{i=1}^r \mathbf{f}^T \mathbf{W} \mathbf{f} + \mathbf{s}^T \mathbf{Q} \mathbf{s} \right\} \quad (2.41a)$$

subject to:

$$\mathbf{T}(\boldsymbol{\alpha})\mathbf{f} = \boldsymbol{\tau} + \mathbf{s}$$

$$\mathbf{f}_{min} \leq \mathbf{f} \leq \mathbf{f}_{max}$$

$$(2.41b)$$

Chapter 3

Experimental Platform

milliAmpère is an experimental prototype developed by NTNU. The ferry serves as an important testing platform for research in the field of autonomous marine vessels. The development of milliAmpère started in 2017.

3.1 Concept

The prototype milliAmpère is a small autonomous passenger ferry designed and developed by NTNU. The ferry is a small vessel suitable for use in canals. The main idea is to provide a new transportation service across water. Many places lack the infrastructure in form of bridges to easily connect different parts of cities or communities. This solution will serve as a cheap, environmentally friendly and non-intrusive solution to this problem. The ferry will therefore serve as an excellent substitute to bridges. The prototype milliAmpère has been made in 1:2 scale. For SysML diagrams that provide more in detail overview of information flow and data structures on milliAmpère, see Appendix B.

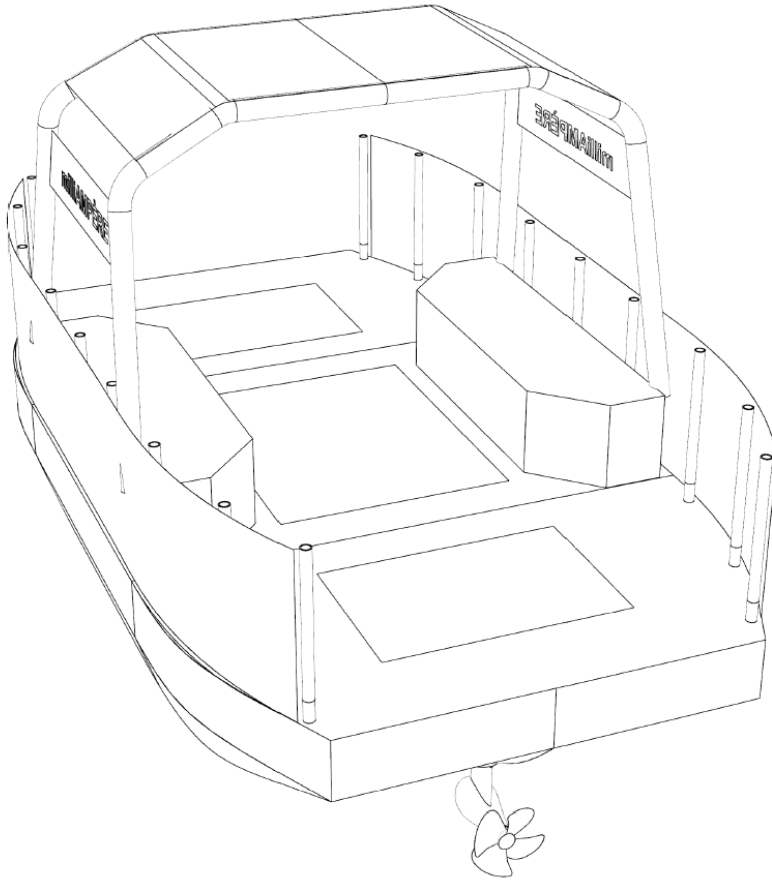


Figure 3.1: Design of milliAmpère. Courtesy of Jon Boye Andresen, Innovation JBA

3.2 Components

The ferry relies on two separate sensors for the motion control system. The main sensor is the Vector VS330 GNSS Compass (Hemisphere, 2018). This component measures the position, velocity and heading data used in the control system. The second sensor is an Inertial Measurement Unit (IMU) from XSSENS (XSSENS, 2018). The IMU provides acceleration and attitude data for the vessel. The GNSS and IMU are mounted at approximately $\mathbf{r}_{gnss}^b = \mathbf{r}_{imu}^b = [0, 0, -1.95]^T$ in relation to the vessel COG. The measurements are transformed into the vessel COG before use.

The prototype has two thruster pods for propulsion, one in the stern and one in the bow. The thruster model used is the Pod Cruise 1.0 from the maker Torqeedo. Each thruster has a power of 2 kilowatts. The resulting output force from each thruster is $400N$. The

thruster pods configuration is shown in Figure 3.2.

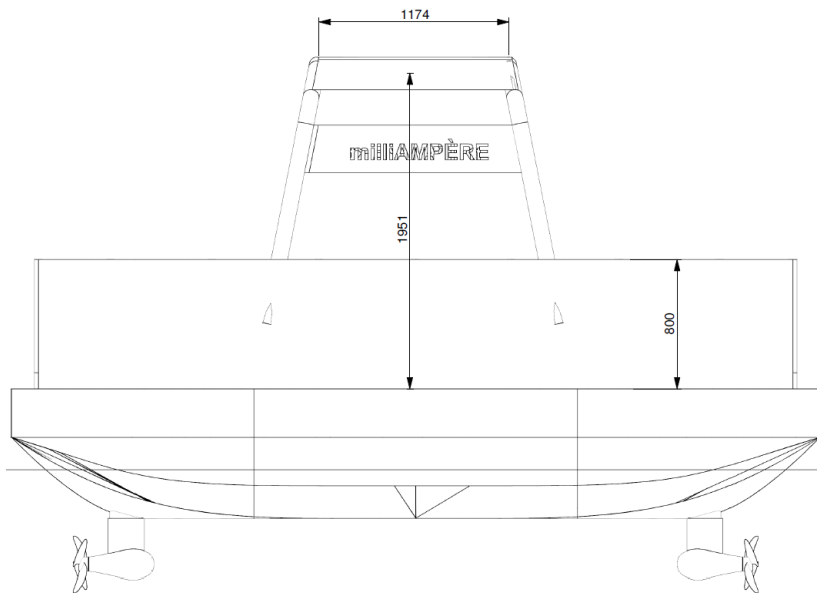


Figure 3.2: Thruster configuration on milliAmpère. Courtesy of Jon Boye Andresen, Innovation JBA

For the control of servo angle, a Brushless Direct Current (BLDC) motor from Intecno is used. The servo is responsible for rotating the thruster to the correct angle specified by the control system. This servo uses a signal voltage of $-10V - 10V$ to control the angular position of the servo. The signal voltage applied is the output from a PD controller. An Ethernet Input/Output (I/O) module is used to generate the desired signal voltage. The PD controller utilizes the angle measured by the absolute encoder as feedback.

The absolute encoder from Wachendorff provides the angular readings used in the feedback. This absolute encoder measures the angular position as well as the number of full rotations performed. The data that provides the number of full rotations is essential to preserve the condition of the power supply and wiring to the Torqeedo thruster from the main power- and control system.

The angular encoder uses the Synchronous Serial Interface (SSI) communication protocol to communicate with an Arduino Mega, which uses bit banging to transfer the bytes containing the angular data. The Arduino transmits the data to the On Board Computer (OBC). Figure 3.3 shows the relevant components.



(a) Torqeedo Thruster Pod (Torqeedo, 2018)



(b) Vector VS330 GNSS Compass (Hemisphere, 2018)



(c) XSENS MTi 10-series IMU (XSENS, 2018)



(d) Arduino Mega (Arduino, 2018)



(e) Wachendorff WDGA36 SSI (Wachendorff, 2018)



(f) Intecno BLDC Wormgearmotor (Intecno, 2018)

Figure 3.3: An assortment of important components in the control system

3.3 Previous Work

The ferry has been developed by NTNU through student summer projects during the summer of 2017 and 2018. The author has taken part in the project during both summers. During the summer of 2017, the main focus was on the building process. All the different components, wires and accessories were installed. Since most of the components were not designed for the specified usage on milliAmpère, custom software drivers for the components were designed. At the end of the summer, the ferry was fully operational with manual remote control. The initial set of sensors needed for autonomous transit was installed and interfaced. As discussed in the previous section, this included high precision Real Time Kinematics (RTK)-GNSS and an IMU. These sensors provides a number of different measurements that are used in the control system. The RTK-GNSS provides the following

- Longitude and latitude, $[l, \mu]$
- Heading, ψ
- Speed over Ground, m/s
- Course over Ground, χ

and the IMU provides

- Gyroscope, $[p, q, r]$
- Accelerometer, $[u, v, w]$

To see more information on these measurements in regards to notation, see Table 2.1. These measurements are used and transformed into the relevant reference frames for use in the system. See Section 2.1 for more details about the transformations. These measurements provides the necessary data for autonomy without collision avoidance.

During the summer of 2018, the focus shifted to software development and software architecture. During that time, the thrust allocation, DP controller and Graphical User Interface (GUI) were developed and implemented on the ferry. See Appendix C for a detailed view of the GUI. The ferry has gone through testing and experimental results were promising. The DP controller implemented over the summer was a basic DP controller with no observer, no model-based feed forward or no wind feed forward. Despite this, the DP controller is quite robust.

To test the accuracy of a DP controller, a 4 corner test is often used. A 4 corner test is conducted by having a square shaped positional reference with different attitude references. A visualization of how a 4 corner test is performed is shown in Figure 3.4.

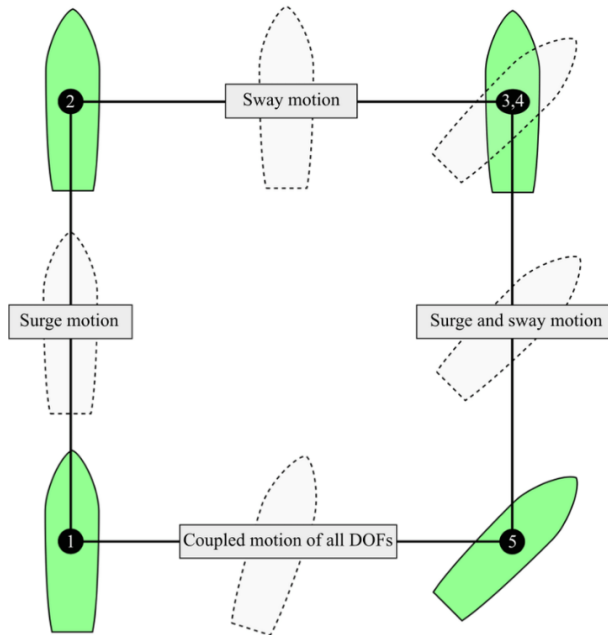


Figure 3.4: Concept of 4 corner test for DP controller. Courtesy of (Lyngstadaas, 2018)

The 4 corner test was performed under good conditions. The result is shown in Figure 3.5. The main issue with the DP controller was lack of heading stability. As a consequence, parts of this project is spent investigating other potential control algorithms to redeem the shortcomings of the already established DP controller.

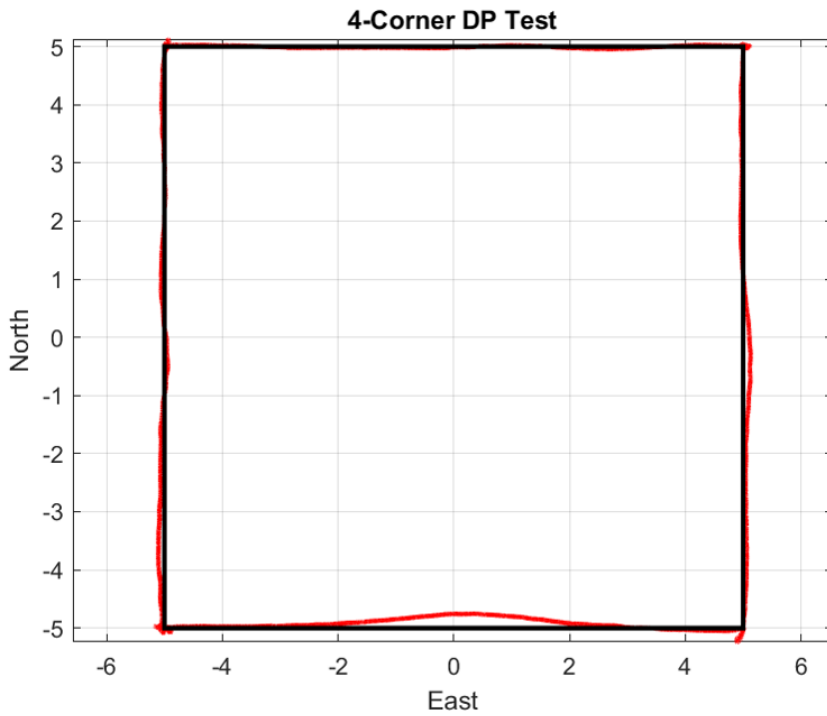


Figure 3.5: Previously performed 4 corner DP test

In Figure 3.6, the measurements are separated into individual plots. The positional accuracy in north and east were spot on, but the heading struggled to stay on the reference when $\dot{\psi}_d \approx 0$. It is important to note that these results were obtained under pristine conditions.

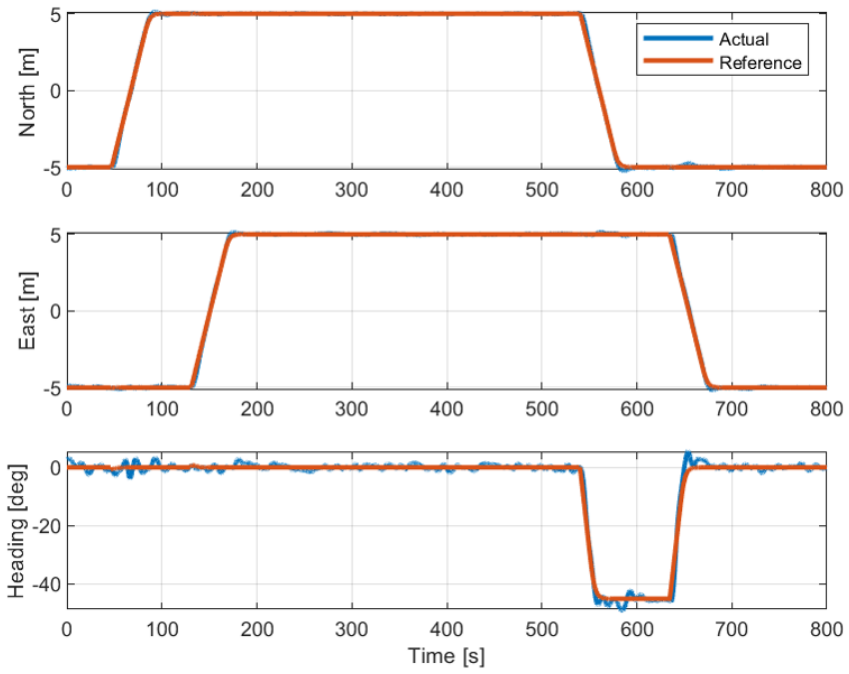


Figure 3.6: Response from individual measurements during 4 corner DP test

Control Design

The two controller design on the ferry depends on which controller is providing the input at any given time. The different controllers are a DP controller, a LOS controller and a surge controller. All the controllers rely on state feedback to compute the error state. The different design aspects and their implementations are discussed further in this chapter. Furthermore, Figure B.6 shows the overall flow of sequences in the motion control system.

4.1 Reference Models

The two different reference models in the system are introduced in Section 2.3. These are a velocity reference model and a pose reference model. It is very important that the generated references are comfortable for humans. According to (Hoberock, 1976), comfortable acceleration for humans during transportation in non emergency situations is in the range of $0.11 - 0.15 \text{ m/s}^2$. With this in mind, the reference models are examined further in this section.

4.1.1 Pose reference Model

The pose reference model is based on the characteristic behaviour of the vessel. It is important to keep in mind that the vessel should be comfortable for humans to stand on, and this has to be part of the constraints for reference trajectory. The reference model is discussed in more detail in section 2.3. The parameters are based on the damping constants and natural frequencies of the vessel. They are given by the diagonal matrices

$$\Omega_p = \begin{bmatrix} 0.5 & 0 & 0 \\ 0 & 0.5 & 0 \\ 0 & 0 & 0.5 \end{bmatrix} \quad \Delta_p = \begin{bmatrix} 1 & 0 & 0 \\ 0 & 1 & 0 \\ 0 & 0 & 1 \end{bmatrix} \quad (4.1)$$

The max velocity and acceleration constraints for the DP controller is set by $\dot{\eta} = [0.25, 0.25, 0.05]^T$ and $\ddot{\eta} = [0.1, 0.1, 0.05]^T$ respectively. The acceleration and velocity constraints are enforced by the use of (2.15). For the accelerations constraints, $\|\ddot{\eta}\| = 0.15 \text{ m/s}^2$. This is within the comfortable region specified earlier.

To validate that the reference model generates a feasible reference for the vessel, a simple test is carried out by simulating the step response for a desired pose reference. The generated references for the pose, velocity and acceleration are shown in figures 4.1-4.3 below.

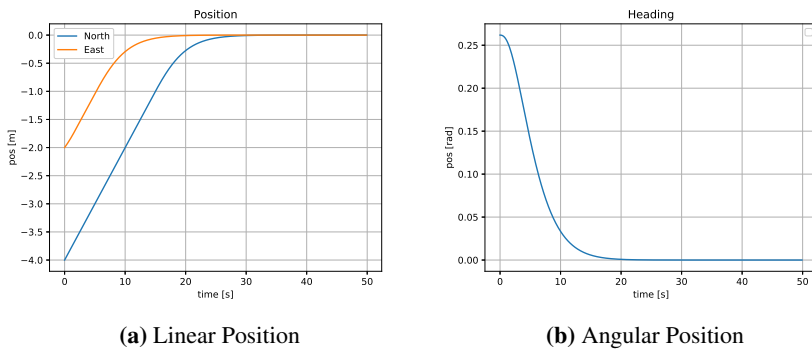


Figure 4.1: Position generated by the pose reference model

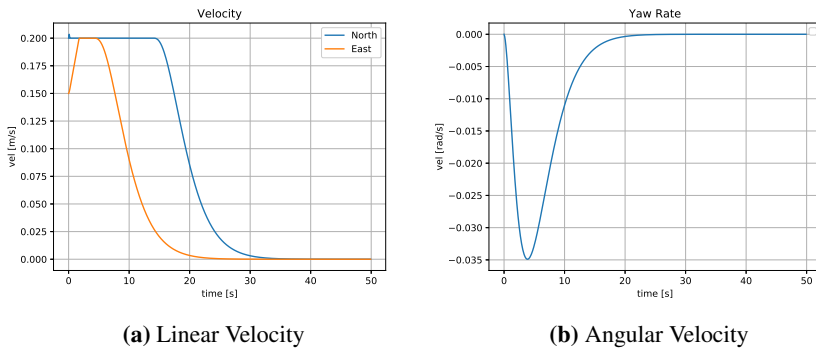


Figure 4.2: Velocity generated by the pose reference model

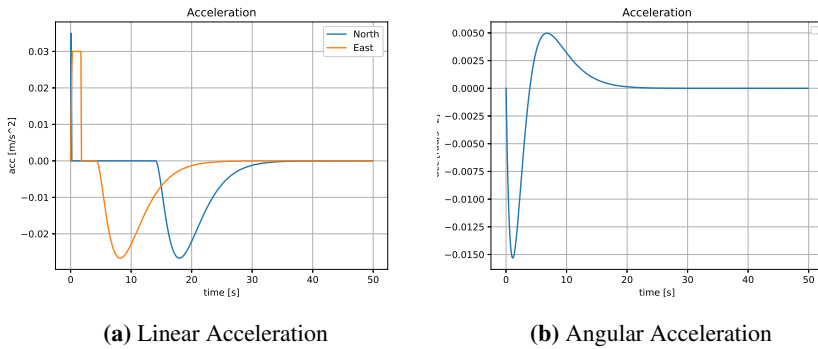


Figure 4.3: Acceleration generated by the pose reference model

In Figure 4.1 and Figure 4.2, the initial conditions are given by $\boldsymbol{\eta} = [-4, -2, \frac{15\pi}{180}]^T$ and $\dot{\boldsymbol{\eta}} = [0.2, 0.15, 0]^T$. This is based on realistic initial conditions in a real scenario. The reference model generates a smooth feasible pose trajectory.

4.1.2 Velocity Reference Model

For the velocity reference model, the same procedure is followed. The reference model is only used for surge speed such that the parameters for the model given by (2.18) becomes constants. To accommodate the acceleration constraints, the velocity reference model parameter values are set to

$$\Omega_v = 0.5$$

$$\Delta_v = 1$$

The intention is to uphold the constraint $\|\ddot{\boldsymbol{\eta}}\| \leq 0.15m/s^2$. The generated step response for the velocity reference model is shown in Figure 4.4.

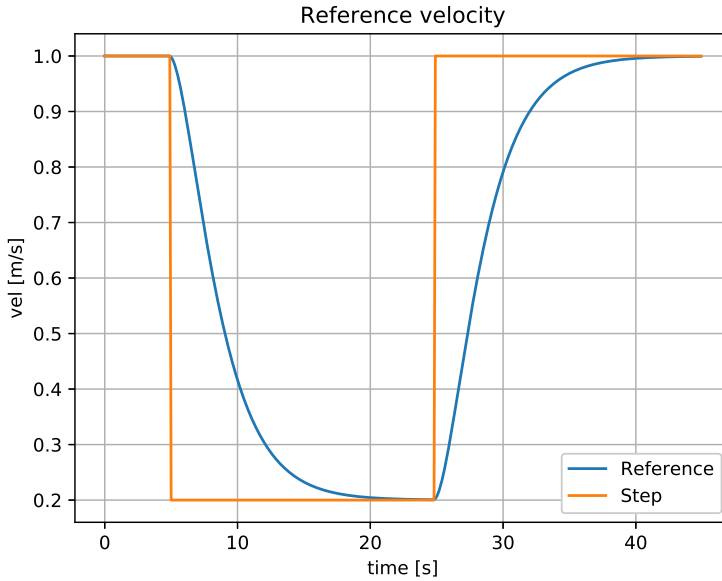


Figure 4.4: Generated surge velocity reference

The current parameters will generate a velocity reference that has a maximum acceleration of $0.148m/s^2$. This is within the specified comfortable region for humans.

4.2 Control Algorithms

The different control algorithms have to be designed differently. This section discusses the different design parameters and highlights other design aspects for the different controllers.

4.2.1 Surge Controller

The velocity controller discussed in section 2.4.2, is only applied in one DOF to control the surge of the vessel. This will simplify the structure of the velocity controller. The control law then becomes

$$\tau_u = m[\dot{u}_d - K_p(u - u_d) - K_i \int_0^t (u - u_d)d\tau] + d_1 u + d_2 |u|u \quad (4.2)$$

The latter terms are part of the model based feed forward, and since no accurate model of the vessel exists as of now, these terms are not taken into account going forward. This reduces the control law to

$$\tau_u = m(\dot{u}_d - K_p(u - u_d) - K_i \int_0^t (u - u_d)d\tau) \quad (4.3)$$

Since this controller is used as the LOS guidance system is running, the desired force output is mapped to an input for the propellers. This relationship is described by

$$\tau = K u_c \quad (4.4)$$

where K is some fitted curve describing the relationship between the actuator input u_c and the force output τ . This K was found by performing a bollard pull test to map the forces the vessel exerts given a specific input. Details of this test are given in Section 6.1. Furthermore, a mapping from thruster input to force output is visualized in Figure 6.1.

4.2.2 Dynamic Positioning Controller

The DP controller is a discrete nonlinear controller. The important elements to consider in the implementation of a DP controller, are saturating elements, yaw wrapping and integrator anti windup. In Section 4.1, the saturating elements are accounted for.

The other important element is yaw wrapping. This means that the actual heading and the desired heading are kept within their defined state of $-\pi \leq \psi, \psi_d \leq \pi$. Integrator anti wind up is discussed in section 2.4.1.

The DP controller is based on the low frequency plant given in (2.29). See Section 2.4.3 for more in depth description of the plant and the DP controller. The implemented DP controller has three uncoupled PID controllers in each degree of freedom. The gain matrices are set to the following diagonal matrices

$$\mathbf{K}_p = \begin{bmatrix} 200 & 0 & 0 \\ 0 & 200 & 0 \\ 0 & 0 & 600 \end{bmatrix}, \quad \mathbf{K}_d = \begin{bmatrix} 700 & 0 & 0 \\ 0 & 700 & 0 \\ 0 & 0 & 1200 \end{bmatrix}, \quad \mathbf{K}_i = \begin{bmatrix} 10 & 0 & 0 \\ 0 & 10 & 0 \\ 0 & 0 & 15 \end{bmatrix} \quad (4.5)$$

The values of the gain matrices in (4.5) can be related to the force outputs from the thrusters. During the DP controller tests, the thrusters had a max force output of $500N$ per thruster. The arm l_x given in Figure 2.7, is $1.8m$. This means that the thrusters can output a maximum of $\tau_{max} = [1000N, 1000N, 1800Nm]^T$ for an uncoupled motion for each separate DOF. For a deviation of

$$\mathbf{e}_1 = \begin{bmatrix} 0.5m \\ 0.5m \\ 0.5rad \end{bmatrix}$$

the desired force output from the proportional gain will be

$$\tau_p = [100N, 100N, 300Nm]$$

The same logic applies for e_2 and τ_d . The τ_i term will continue to accumulate proportionally with the integrated error state $\int_0^t e_1(\tau)d\tau$ with a factor of the relevant entry in the K_i matrix.

4.2.3 Line of Sight Controller

The LOS controller is used during the transit. This controller is chosen because of its heading stability which the DP controller showed to struggle with. By only controlling the rear rudder and the thrust as an under actuated vessel, it will provide an opportunity to ensure better stability of the heading angle.

As in the DP controller, certain design aspects are of importance. This includes accounting for saturating elements as well as yaw wrapping. The saturating element is the maximum allowed angle of the rear rudder. This is set to $\delta_{r_{max}} = \pm 30^\circ$. It is also made sure that the heading is wrapped such that $-\pi \leq \psi, \psi_d \leq \pi$.

LOS

The controller gains for the desired course for the standard LOS controller is given by

$$K_p = \frac{1}{\Delta}, \quad \Delta > 0 \tag{4.6a}$$

$$\chi_r(e) = -\arctan(K_p e(t)) \tag{4.6b}$$

According to (Fossen, 2011), a general rule of thumb for Δ is to choose the parameter in the range of 1.5 to 2.5 of the vessel length. $\Delta = 10$ is chosen going forward. Since the sideslip, β , is compensated for as shown in (2.35), the need for an integrator in the term χ_r is removed. For the LOS controller it is also important to negate the effect of anti windup. This is done by disabling the integral function when the rudder saturates.

ILOS

In addition to the standard LOS controller, an ILOS controller is looked into. This gives the possibility to compare the performance between the two different approaches during real life experiments. For ILOS, the controller needs a bit more care. The K_p gain is still

the same as given in (4.6). However, since it is assumed that the external disturbances are unknown, an integral term is introduced. The new expression for the desired course is

$$\chi_d = \chi_t - \arctan\left(\frac{e + \sigma e_{int}}{\Delta}\right) \quad (4.7a)$$

$$\dot{e}_{int} = \frac{\Delta e}{\sqrt{\Delta^2 + (e^2 + \sigma e_{int})}} \quad (4.7b)$$

where $\sigma = 5$, $\Delta = 10$. Both of the LOS controllers solve the same control objective, but the performance may vary based on how accurate the sideslip compensation is.

The ILOS and LOS controllers calculate a desired heading for the vessel denoted as ψ_d . ψ_d is used as input for the attitude reference model described in section 2.3.1. A PID controller is then used to drive the error state to zero, i.e. $e = \psi - \psi_d \rightarrow 0$.

4.3 Transition State

The transition state is an added state that serves the purpose of handling the necessary preparations before a switch to any of the different controller discussed in section 2.4. The DP controller and its reference model is designed for low velocities and station keeping, so it is important that those conditions are met when the switch to the DP controller is made. If this is not handled properly, large trajectory errors and overshoots may occur. This would result in unwanted behaviour.

The Transition state is triggered by using the circle of acceptance to determine the distances to the different docks. This is defined as

$$[x_k - x(t)]^2 + [y_k - y(t)]^2 \leq R_k^2 \quad (4.8)$$

where x_k and y_k forms the desired position coordinates, $x(t)$ and $y(t)$ is the current position coordinates, and R_k is the radius of the circle of acceptance. By utilizing this, the state machine has the added logic to determine the active controller based on relative position.

The main purpose of the transition state is to control the velocity of which the vessel moves, and that the angle of the azimuth thrusters are correct given the incoming switch. The transition state is a combination of a LOS controller and a surge controller.

4.4 Thrust Allocation

As discussed in Section 2.5, the optimization problem in question is non convex. The characteristics of the azimuth thrusters determines the time delays for applying a certain thrust, and to rotate to a specific angle. This will effect the most efficient way of generating the

desired 3 DOF force output. In other words, it is necessary to penalize certain behaviour. For example, the maximum angular velocity for the thrusters are relatively low. As a consequence, large changes in angles are penalized greatly to discourage changes in angle to achieve a certain force output. The QP problem is formulated as

$$J = \min_{\mathbf{f}, \mathbf{s}, \boldsymbol{\alpha}} \left\{ \sum_{i=1}^r \mathbf{f}^T \mathbf{W} \mathbf{f} + \mathbf{s}^T \mathbf{Q} \mathbf{s} + \Delta \boldsymbol{\alpha}^T \boldsymbol{\Omega} \Delta \boldsymbol{\alpha} \right\} \quad (4.9)$$

subject to:

$$\begin{aligned} \mathbf{T}(\boldsymbol{\alpha}) \mathbf{f} &= \boldsymbol{\tau} + \mathbf{s} \\ \mathbf{f}_{min} &\leq \mathbf{f} \leq \mathbf{f}_{max} \\ \boldsymbol{\alpha}_{min} &\leq \boldsymbol{\alpha} \leq \boldsymbol{\alpha}_{max} \\ \Delta \boldsymbol{\alpha}_{min} &\leq \boldsymbol{\alpha} \leq \Delta \boldsymbol{\alpha}_{max} \end{aligned}$$

Simulation Results

A series of simulations were conducted during the course of the project. This chapter presents the results from these simulations. The simulated environment was also used as a debugging tool. By using it as a debugging tool, the implementations of the different control algorithms could be validated before real life experiments commenced.

5.1 Crossing tests

The simulator was used to carry out crossing tests by simulating two virtual docks at two positions. The waypoints used in these simulations were $\eta_1 = [0, 0, 0]^T$ and $\eta_2 = [60, 60, \frac{45\pi}{180}]^T$. There was also added a constant disturbance to the simulation. The disturbance force was perpendicular to the vessel itself to simulate the current disturbance the ferry will be exposed to in a real life scenario. It is important to note that these simulations were done in a simplified environment. As a consequence, the results are not that accurate. This is deemed acceptable since the controllers is not to perform under the same model parameters used in the simulated environment. Instead, the controller gains were roughly tuned.

By using the simulator, the different switching mechanisms and control algorithms were tested and debugged to make sure that they were implemented correctly. Seeing as it is far more convenient to develop and debug code in an office at a proper desk and work station, the ability to debug code prior to doing the initial experiments on the ferry was invaluable. As stated, the simulated environment is not accurate, so the final tuning must be conducted on milliAmpère.

5.1.1 Simulated Position

Figure 5.1 shows the behaviour of the vessel during a crossing of the canal. The results were satisfactory, and the simulations showed that the implementation is correct. The importance here was that the ferry departed and docked at the specified locations. The black markers in figures 5.1-5.4 signify switching between states in the state machine. The results were very encouraging.

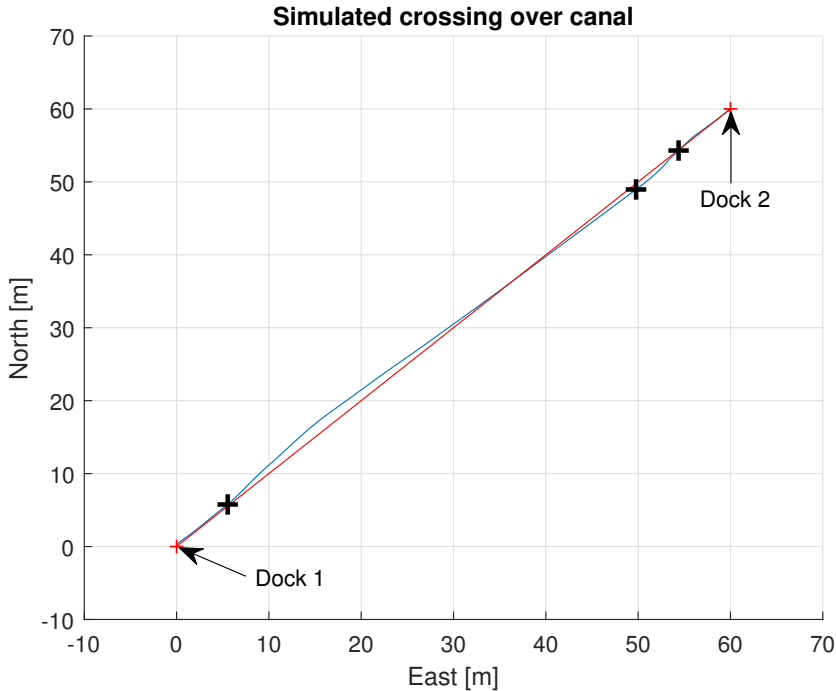


Figure 5.1: Simulation of a canal crossing. Position and virtual docks are shown

The DP controller handles the initial departure and final docking phases. This means that the required heading position as the vessel is positioned by the docks is met. During transit, the LOS controller takes over and controls the heading to be what is desired. While the LOS controller controls the heading, an uncoupled surge controller controls the thruster output. Together they form the control algorithm during the transit. For a visualization of the heading angle of the vessel during crossing, see Figure 5.2 below.

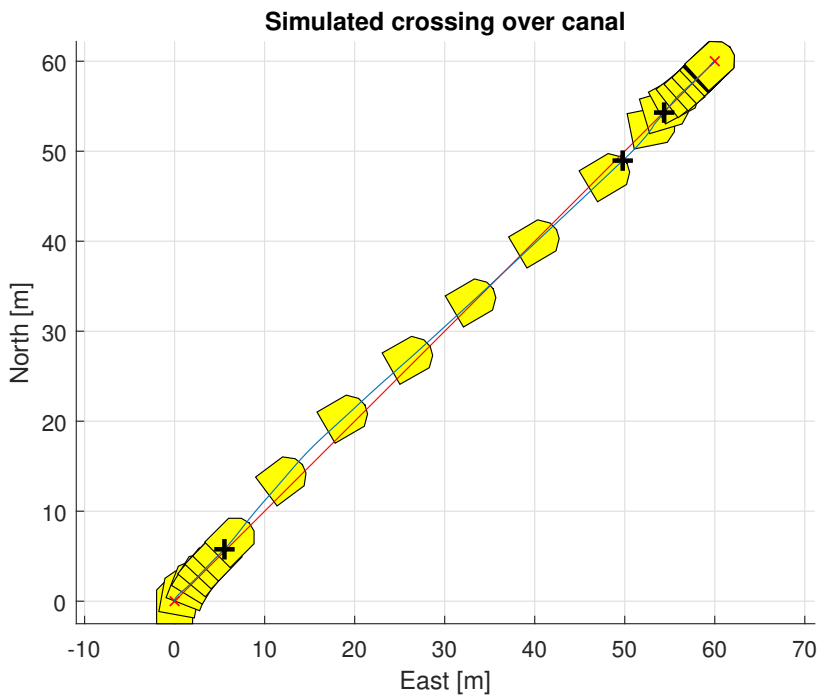


Figure 5.2: Simulation of canal crossing with heading visualization

The ferry correctly has a sideslip angle to compensate for the external disturbances that are present. Additionally, the cross track error is visualized in Figure 5.3. The cross track error goes towards zero as intended.

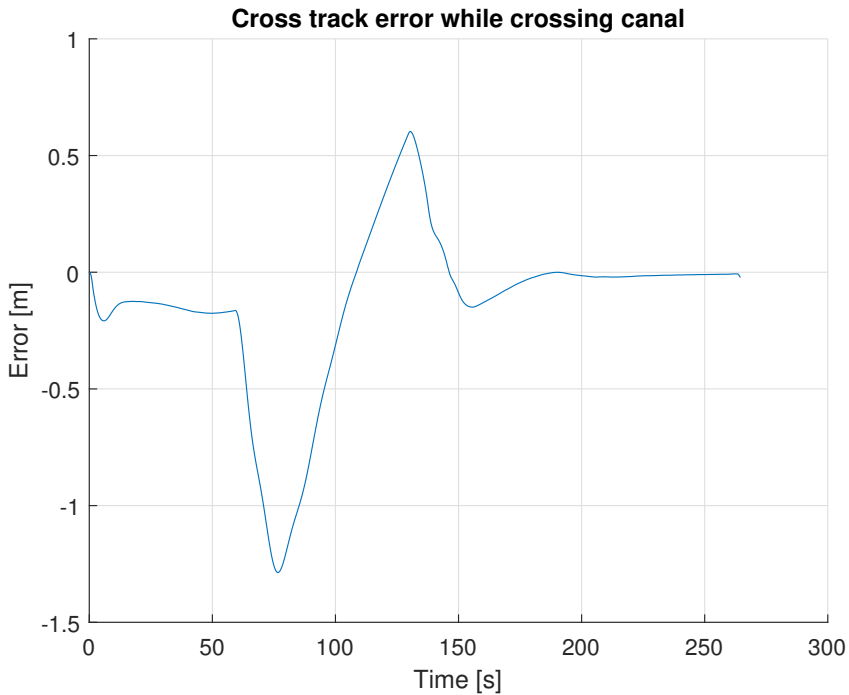


Figure 5.3: Cross track error during simulation of crossing

5.1.2 Simulated velocities

Figure 5.4 shows the velocities in surge, sway and yaw during the different parts of the crossing. The velocity up until 60s is during DP operation. The first black marker visualizes when the state machine invokes a state switch to the transition state. As the velocity stabilizes, the switch has been made to LOS operation. When the velocity decreases, the transition state has yet again been switched to, and the velocity is controlled such that it reaches the desired velocity before DP operation resumes. The DP controller then makes sure the vessel docks properly.

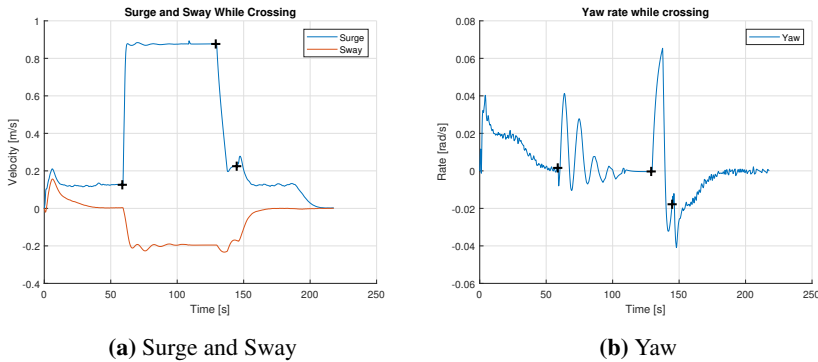


Figure 5.4: Surge, Sway and Yaw during simulated crossing

The most crucial part of the crossing is the switch from the transition state to DP operation. As the DP controller is meant to operate under low velocities, it is imperative that the velocities of the vessel is sufficiently low when DP operation is supposed to commence. Figure 5.4 shows that there are no big jumps in velocity, and that the switch is made successfully. However, there are some minor oscillations in yaw.

5.2 Discussion

The initial simulations showed that the state machine and control algorithms worked as intended. The main control objective was met in a satisfactory fashion. The initial troubles with lack of stability in heading direction, seems to be somewhat sorted out with the use of a LOS controller. This is directly visible in Figure 5.4 as the yaw velocity is very small during transit. There are some small deviations in the simulated results, but this is to be expected as the controllers are not specifically tuned towards the current simulated environment. All in all the results were promising, but it is important to keep in mind that this is a simplified simulator with a model with inaccurate maneuvering characteristics. The final thoughts and conclusions must be drawn from the experimental results that are obtained later.

Chapter 6

Experimental Results

A series of experiments were conducted during the course of the project. This chapter presents the different challenges that were encountered and the results from these experiments. There is also a brief discussion about performing experiments on milliAmpère.

Logistical Difficulties of Testing

The test platform can provide some logistical issues in regards to performing experiments. Given that milliAmpère is a prototype, there are extra precautions concerning normal operation of the vessel. Safety guidelines dictates that at least two people should be on board the ferry at all times in case of malfunction. This puts limitations on available time slots to conduct experiments. Another issue is that milliAmpère serves as a testing platform for other students. This further restricts available testing time. Other limitations such as scheduled demos, weather conditions and hardware issues meant that it was not possible to thoroughly test the proposed solution in the specified time frame.

Malfunctioning interface between Arduino and Absolute Encoder

Another problem that needed addressing, was replacing the solution for reading the absolute encoder. One of the Printed Circuit Board (PCB)'s that served as the hardware interface between the arduino and the absolute encoder, had malfunctioned. As a result, a new solution was designed. Both the PCB's were scrapped, and the new solution was to use an arduino shield to provide a simple, space saving and robust bit banging interface between the arduino and the absolute encoder. This was developed by the author at the beginning of the project. The schematic for the arduino shield is found in Appendix D.

Broken Propeller

The ferry was shipped to Haugesund to be present during Sjøsikkerhetskonferansen. During these days, the ferry showcased its capabilities for autonomous docking. For milliAmpère to be in Haugesund was significant. Autonomous vessels introduce a number of new challenges concerning safety and operation at sea. Introducing milliAmpère to the public, as well as the legislators of marine safety, is an important part of promoting the use of vessels similar to milliAmpère.

After transportation from Haugesund and back to Trondheim, the first major problem was encountered. During the transportation one of the propellers broke. The broken propeller was replaced, and new propellers were fitted to the ferry. The new propellers did not have the same characteristics as the old ones. To correct for the new behaviour, a new bollard pull test was performed. This was unfortunate as it demanded extra tests to uncover the new behaviour. The necessary tests put even more strain on the existing time constraints.

6.1 Bollard Pull Test

The bollard pull test was performed by tying a weight to the stern of the ferry. By using a series of steps on the input to the thrusters, the resulting force the ferry exerted was recorded. This test resulted in a new mapping from thruster input to force output. The result from the test is plotted in Figure 6.1. The parameters found to fit this mapping was of a 5th order curve fit.

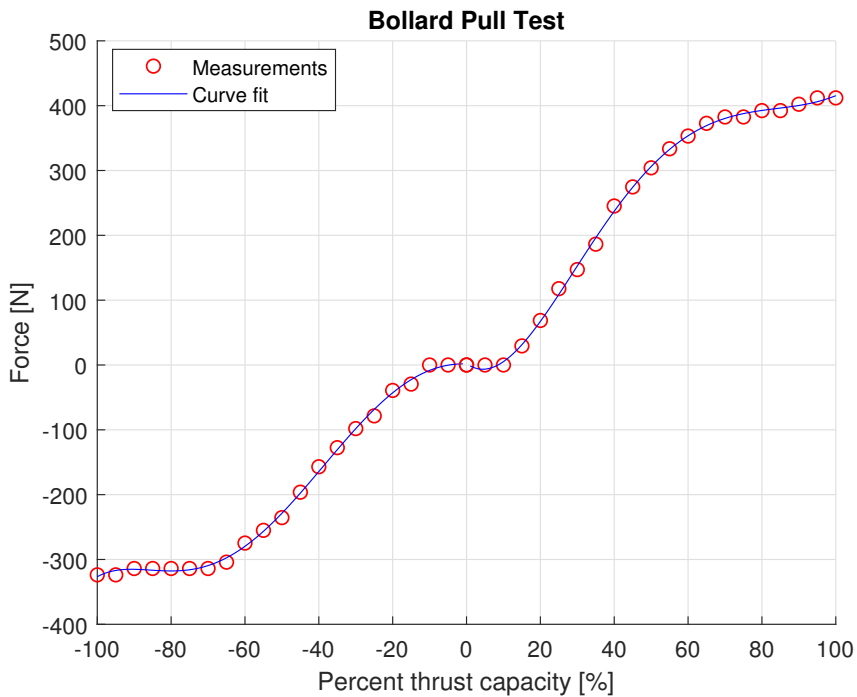


Figure 6.1: Mapping from percentage of thrust capacity to generated thrust force

6.2 Test Area

Trondheimsfjorden was declared the first test site for autonomous ships in the world in 2016 (Sae-Khow, 2016). A natural place to test the new implementations on the ferry was Havnebassenget by Brattøra. It is important to have big safety margins as the ferry is a prototype and has no backup solution. Given the severity of the situation if a crash is to occur, a big open area is favorable. As the traffic in this area is minimal, it serves as a perfect testing area for the ferry. The ferry is normally moored inside the canal by the Trondheim Railway station. The ferry is moved under manual control to Havnebassenget for testing.

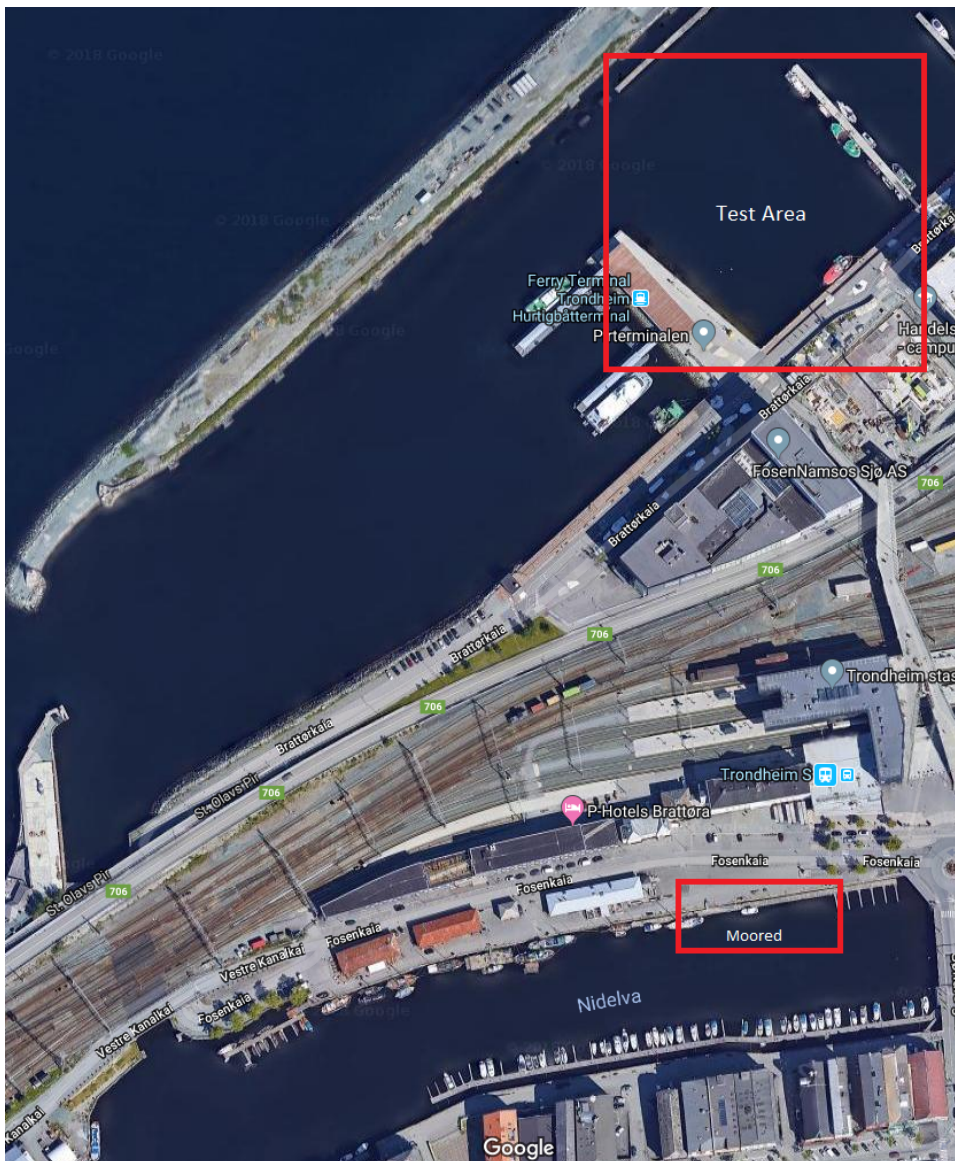


Figure 6.2: Test Area for milliAmpère

6.3 Experiments the 30th of November 2018

6.3.1 Conditions

Clear sky

Wind: 8-10 m/s

The conditions started out calm. However, as the day passed noon, the wind picked up considerably. Unfortunately, the wind got so strong that the conditions were deemed unsafe. The experiments were cancelled and rescheduled.

6.3.2 Intentions

The intentions for the experiments were to tune the newly designed control algorithms on the ferry. The main goal was to optimize path and velocity accuracy based on the pre-defined trajectories. To expose any weaknesses, each individual part of the crossing was subjected to isolated tests during the experiments. The intended purposes of the experiments are summarized in the bullet points

- Test the new bollard pull parameters and response from the newly fitted propellers
- Test velocity transform from GNSS to COG
- Find tuning parameters for the various PID controllers
- Determine parameters for comfortable acceleration and deceleration in transition state
- Determine optimal thrust configuration for thruster force in transition state to ensure comfort and accuracy
- Perform performance tests on accuracy for position, direction and velocity and the errors involved

6.3.3 Execution

The new implementations included many lines of code that the simulated environment did not employ. It was imperative to set aside enough time to sort out the minor bugs in the code still present.

The initial testing validated the new implementation of the velocity measurements from the GNSS. The transform from the GNSS antennas to the COG, needs further examination. This was not working as it should have.

Next was the test of the DP controller and the new thrust allocation parameters. By executing a quick performance test, the DP system showed prowess by holding the specified reference position with an accuracy of 20cm. The new parameters for the input/output thrust relationship was deemed satisfactory. However, the stability in heading was not up

to par. The new propellers behave differently and have a different response than the original propellers. This causes unwanted behaviour for changes in the desired thrust output. The new characteristics of the propellers are different, and additional tests to uncover the new DP controller gains are necessary. The old propellers are scheduled to be refitted in the near future, so the DP controller was left as it was.

The intention of the first initial crossing experiments were to tune the new controller parameters. The first experiments uncovered deviations from the intended path, and the gains in the relevant controllers were adjusted accordingly. After different experiments with different parameters, the ferry successfully made a crossing, albeit with a considerable cross track error. The issue was that the surge controller did not provide enough thrust to allow the heading controller to correctly guide the vessel towards the predefined path.

As experiments to improve the surge controller were about to start, the wind picked up to the point where the conditions were unsafe. The rest of the experiments were cancelled and rescheduled.

6.3.4 Reflections

What these experiments revealed was that the vessel was difficult to control under rough wind conditions. However, the DP controller did a reasonable job. The controller could directly produce a force vector in any direction to counteract the various external disturbances. This raised some questions as to how well an under actuated controller solution can guide the vessel under rough conditions. Given the shallow hull and big surface area above the waterline, milliAmpère proved to be alarmingly susceptible to wind disturbances. Since this kind of controller is not able to directly counteract the forces the surroundings exerts on the vessel, large external disturbance are of concern. However, more experiments were planned as soon as the weather looked promising. Proper tuning may vindicate the initial suspicions these experiments raised.

6.4 Experiments the 6th of December 2018

6.4.1 Conditions

Clear sky

Wind: 0-4 m/s

The morning started out a bit choppy with some wind coming from the south. The wind was considerable, but provided no safety issues. The experiments began as soon as the daylight allowed it. The wind died down approximately at noon, and the conditions were pristine as the day passed 13.00.

6.4.2 Intentions

The intention for the experiments was to continue tuning the parameters for the different control algorithms. The intended experiments served the purposes summarized in the bullet points

- Continue tuning the gains for the various PID-controllers
- Determine velocity reference model parameters for proper acceleration and deceleration
- Perform performance tests on accuracy for position, direction and velocity and the errors involved
- Determine a suitable thrust configuration in the transition state

6.4.3 Execution

Initial tests were conducted to verify the results achieved on the tests performed on the 30th of November. After the results were verified, the experiments planned for the day commenced.

The first experiments were done while stationary and moored to the dock. The purpose was to test different parameters in the controllers. By staying stationary and observing the desired output, multiple parameters were easily tested in a short period of time. This allowed to quickly find controller parameters that produced both feasible and reasonable outputs. Using the parameters found by this method, the full scale experiments for the heading and surge controller began.

The first tests were performed with a constant thrust and only LOS control. By performing the test this way, the heading controller was isolated. This made it easier to tune the heading controller. Although the gains found were suboptimal, they were deemed satisfactory considering the given time frame.

The next tests centered around the surge controller. After successful tests making the surge controller behave nicely, the focus shifted towards testing of different thruster configurations. The different thruster configurations were tested during the stage of deceleration. Unfortunately, proper thorough testing was not possible as another student needed to conduct his experiments before daylight ran out. As the second day of testing came to an end, the various controllers behaved decently. Although more time to adjust parameters would've produced better results, the circumstances simply didn't allow it.

6.4.4 Reflections

The first successful experiments were performed this day. The strength and weaknesses of this solution was now apparent. Most apparent for the proposed solution, was how hard it was to decelerate before the ferry was supposed to dock. Given the characteristics of high maneuverability of the ferry, the heading was hard to accurately control as acceleration

and deceleration occurred. Moving forward, the stability in heading is the biggest concern. These experiments revealed that utilizing a path following control algorithm like LOS in a small confined area was troublesome for milliAmpère.

6.5 Results

The results obtained through experiments are represented in figures 6.3 - 6.11. The progression of the figures follows the progress that was made during the experiments. The black markers on the various plots represent the switch between different states and consequently the different control algorithms used by the system.

6.5.1 Initial Crossing Tests

The first initial tests showed a lack of ability to converge to the desired path fast enough during transit. The gains for the heading controller was adjusted accordingly to alleviate the experienced error. As seen in Figure 6.3, considerable problems arose when the switch from transit to docking was made. This switch is visualized by the black marker positioned roughly at $[N, E] = [-30, -30]$.

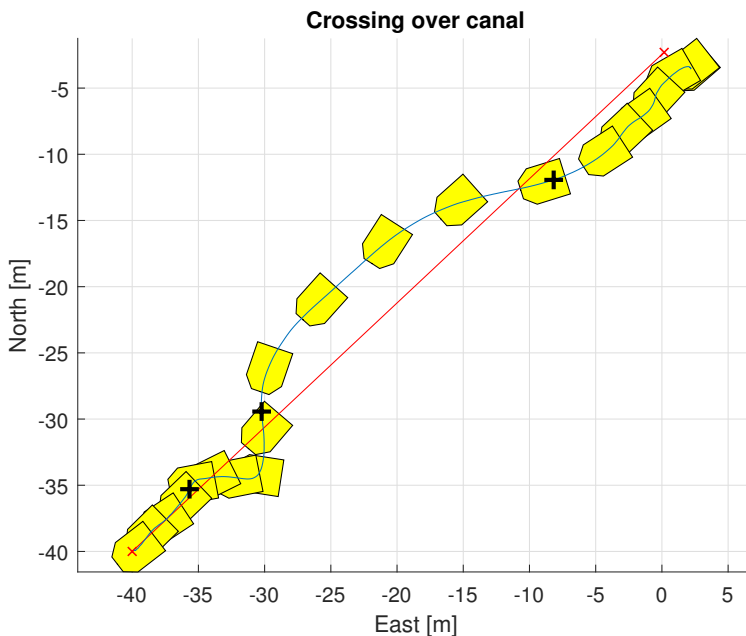


Figure 6.3: First crossing test, Pose

The first initial tests tried decelerating using natural damping in the environment. The main idea was to ensure smooth deceleration while consuming minimal amount of power. The first approach was to maintain a small thrust force on the rear thruster to control the heading, and no force on the front thruster. What this approach showed was that having a balance between the desired heading and decelerate at the desired pace, was not possible. Different velocity reference model parameters were tried, but none gave a result that was satisfactory. Plots showing the velocity response and cross track error during one of the experiments are visualized in figures 6.4 and 6.5 respectively.

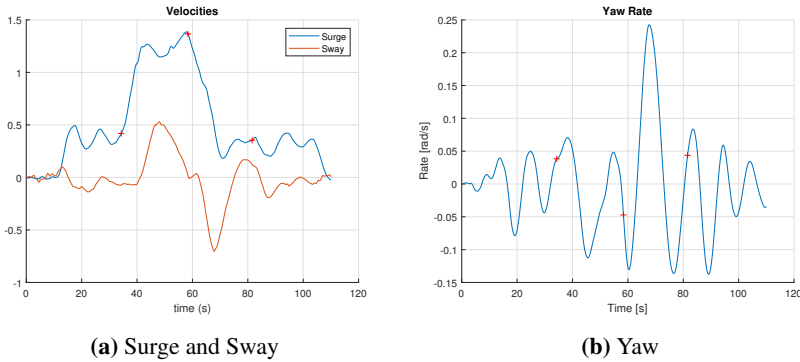


Figure 6.4: First crossing test, Surge, Sway and Yaw

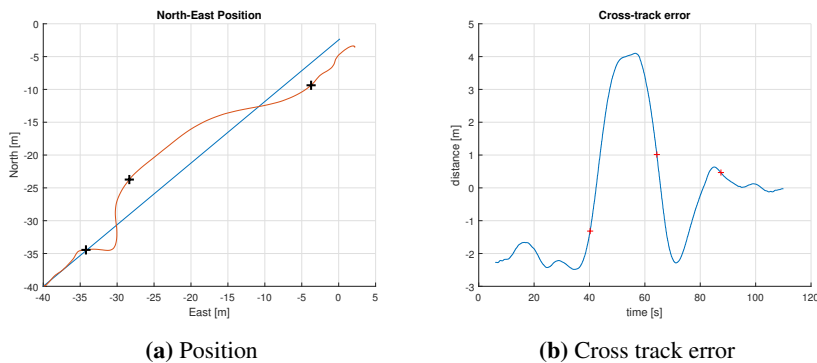


Figure 6.5: First crossing test, Position and cross track error

Another approach tested was to only produce an output force perpendicular to the desired path, but this approach was abandoned since the natural deceleration was too slow. The approach of using the natural damping in the environment was abandoned due inability to maintain desired heading. In the upcoming experiments, a different approach was explored.

6.5.2 Different Thrust Configurations

Given the first initial experiments, it was evident that slowing down by means of natural damping in the environment was not a suitable solution given the spatial constraints. The next approach explored the possibility of using the rear thruster for heading control, and the front thruster as surge control. This was achieved by using the two thrusters separately. The front thruster had a constant thrust force while operating like a rudder. The front thruster on the other hand was fixed in the neutral position, and was only allowed to exert a varying force along the x-axis in the BODY frame. The front thruster used the surge controller to calculate the desired force output. The results from the first initial experiments using this strategy is showcased in figures 6.6-6.8.

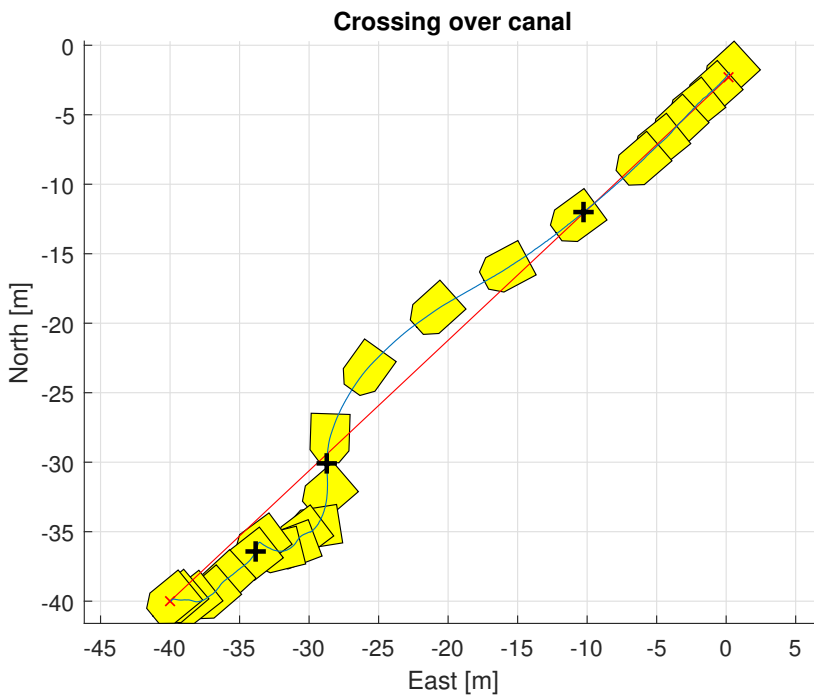


Figure 6.6: Second crossing test, Pose

By using this strategy, more flexibility was allowed as the desired deceleration was independent of the heading control. By not limiting the ability for heading control, the results were better. Although, this strategy was promising, it was obvious that the control algorithm parameters needed further tuning.

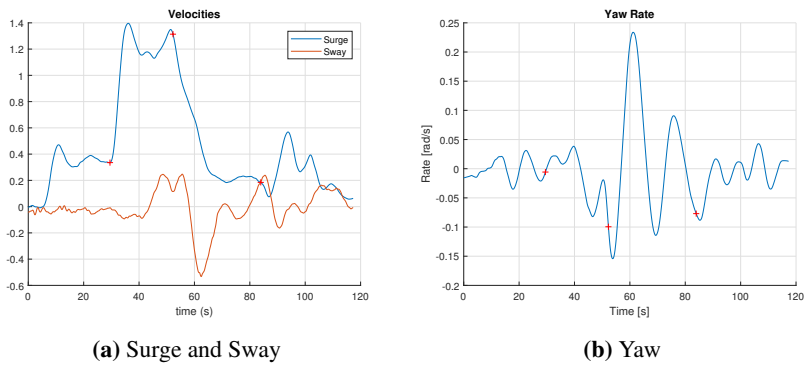


Figure 6.7: Second crossing test, Velocities With Velocity Reference Model

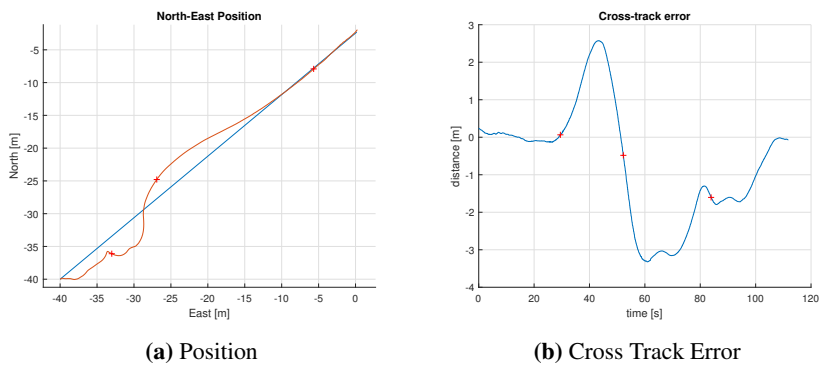


Figure 6.8: Second crossing test, Position and Cross Track Error

6.5.3 Tuning of Velocity Reference Model and Surge Controller

By adjusting the parameters in the velocity reference model and surge controller, positional accuracy improved. The result is shown in Figure 6.9.

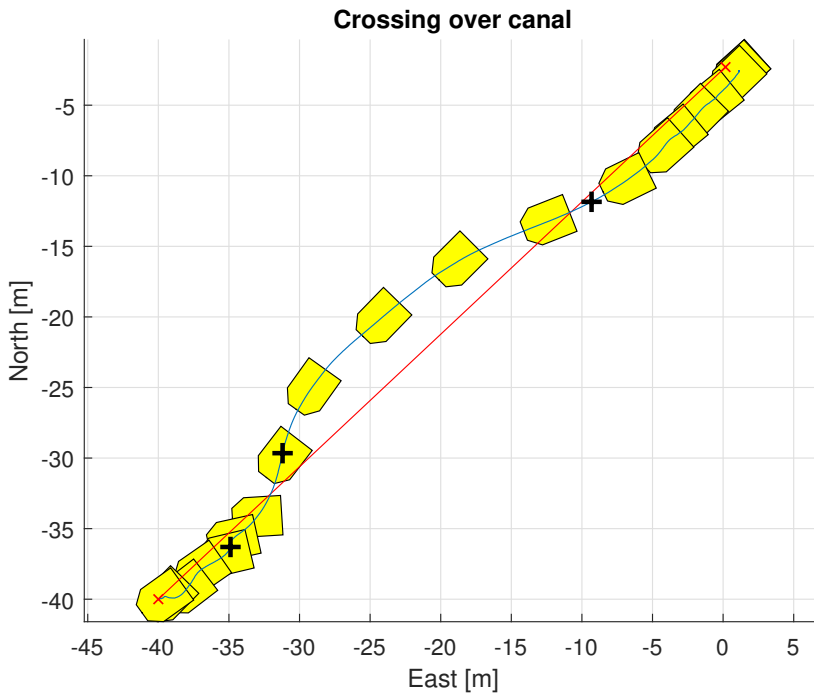


Figure 6.9: Third crossing test, Pose

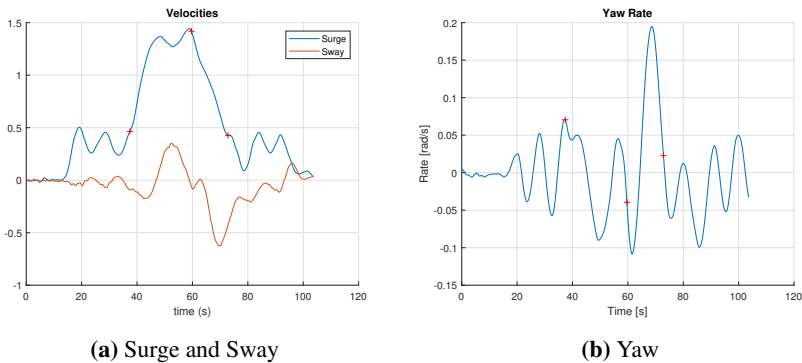


Figure 6.10: Third crossing test, Velocities

Figure 6.7 shows that the desired surge speed was reached well before the switch to the DP controller. To force slower deceleration, the velocity reference model parameters were relaxed. By adjusting these parameters, the deceleration followed a more suitable trajectory with softer deceleration. Figure 6.10 shows the velocities obtained with the use of the new parameters. The positional accuracy did improve, however the biggest flaw of

oscillation in heading position was still present. Given more time and more testing, the accuracy would've improved. However, overcoming the heading instability experienced with this approach seemed unlikely.

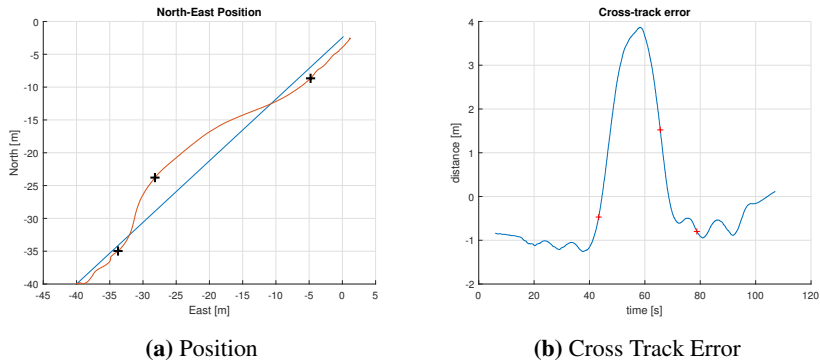


Figure 6.11: Third crossing test, Position and Cross Track Error

The intention was to test some other thruster configurations during the transit and deceleration phase, but there was not enough time to be able to perform all the tests that were planned.

Discussion

This project provided valuable lessons and insight for further development of milliAmpère. This chapter serves to highlight some remarks about the execution of this project. Some other important aspects of the project are also discussed.

7.1 Time Challenges

The time constraint was of concern during the entirety of this project. When going into this project, this was an important part of the planning. As the possibility for continuous experimental tests was possible, these were planned to sustain progress. It was made a point to act on the strategy of continuous testing going through the semester. One major inconvenience was the schedule of demos that were planned for milliAmpère. In between the shipping of the vessel to Haugesund and making sure that the vessel was ready for the scheduled demos, milliAmpère was unavailable for testing up until the 7th of November.

Given the unavailability of milliAmpère, the plan for continuous testing was scrapped. As a result of this, all aspects of the planned solution was implemented before experiments were conducted. This was problematic as the shortened time frame would make it difficult to conduct sufficient amount of testing and tuning. Further damages to the propulsion system meant that another bollard pull test was performed. This was also unfortunate as an entire day designated for testing was lost. Unforeseen events and hardware issues sadly had an negative effect on the end results in this report.

Other aspects of testing also had a negative impact. The main problems were the need for multiple people to conduct experiments. Since the people involved were working on different projects, finding time that suited both parties was an added obstacle that restricted the amount of time for testing. This also meant that all parties had to assist in work that

didn't relate to their respective projects. In an otherwise busy time of year, this led to further restrictions.

7.2 Solution

The implementation of the intended solution was partly successful. The main control objective was solved, but the accuracy of the motion control system was suboptimal. There was implemented different solutions to solve the problems in the deceleration phase. This was already planned ahead as the simulated environment provided data to showcase the difficulty of this task. This led to the implementation of different thruster configurations for this phase. This was discussed in more detail in section 6.5.2. If these configurations weren't planned ahead, the given time frame may have inhibited the ability to produce results.

The thrust configuration of using the front thruster as surge control showed prowess for the task at hand. However the small area the ferry is allowed to operate in, and thus the need for harder deceleration, made it difficult to achieve great accuracy. The issue of general instability in heading position didn't help. It is also important to note that the newly fitted propellers require updated gain matrices in the DP controller. The original propellers are planned to be refitted since they had better performance overall. Given this knowledge, the gains for the DP controller was left untouched to spare time. The oscillations while in DP operation are therefore larger than normal.

There were also minor issues with switching between controllers. The ferry was very sensitive to small yaw moments. The issue of small perturbations while switching between different control allocations resulted in some unwanted effects. Most noticeable was the small delay that allowed the yaw moment to perturb the heading position slightly of course. This was difficult to remedy in the short distance the ferry traveled.

An important final note was that the vessel was highly susceptible to external wind disturbances. The advantage with heading stability for the LOS controller was irrelevant when the external disturbances forced the vessel off course. Given the initial data obtained through the experiments performed, it became apparent that a fully actuated control solution should be investigated.

Conclusions and Future Work

8.1 Conclusions

In this report further implementations for autonomous transit and docking are carried out. The main goal of remedying the issues with heading instability showed through DP operation is looked into. The vessel has high maneuverability suitable for confined environments, but not without the price of heading instability. The initial testing with a LOS controller proved to improve heading stability during transit. However, the benefits of this solution brought unwanted challenges with it. The ability to maintain high accuracy was not achieved. The LOS controller had a cross track error of 3-4m. Given time for tuning, this will improve.

The unique design of milliAmpère makes it highly susceptible to external disturbances. A big concern with the LOS controller is the inability to counter these external disturbances in a timely manner. This is an important lesson, as it shows that a fully actuated solution could potentially serve as the best alternative for better overall performance.

A challenging part of the project was the inability to perform experiments frequently. Performing experiments meant to identify multiple issues at once, made the experiments unnecessary hard and complicated. Although higher accuracy and better performance for the implemented solution was desired, the implementation worked as intended. Some important lessons were learned during the project. The nuances of the behaviour of the vessel and better knowledge of other potential solutions will prove indispensable moving forward.

The addition of a simulated environment proved extremely useful. Online testing on the ferry was time consuming, and the ability to perform simple tests in the simulated environment was invaluable.

The last important lesson learned was the need for planning and preparation. During the

course of the report, too much time was spent on developing and working on solutions that yielded no contributions in the end. This highlighted the importance of proper planning and thorough research. In future work, this will become a priority.

8.2 Future Work

The approach pursued in this report yielded decent results that solved the problem at hand. The work done provided valuable insight and base knowledge for further development. The thoughts and ideas for future work in the MSc thesis is summarized by

- Investigate different trajectory following motion control strategies
- Implement an observer for the navigation system
- Implement an adaptive trajectory following controller to handle relevant scenarios, external disturbances and modelling uncertainties.
- Perform real life experiments to ensure robust and accurate motion control

Bibliography

- T. I. Fossen, *Handbook of Marine Craft Hydrodynamics and Motion Control*. John Wiley & Sons, 2011.
- M. Breivik, "Topics in guided motion control of marine vehicles," Ph.D. dissertation, Norwegian University of Science and Technology, Trondheim, Norway, 2010.
- O. N. Lyngstadaas, "Ship motion control concepts considering actuator constraints," Master's thesis, Norwegian University of Science and Technology, Trondheim, Norway, 2018.
- WGS84, "Wgs84," <https://gisgeography.com/wgs84-world-geodetic-system/>, Last Accessed 14.12.2018, 1984.
- SNAME, "Sname1950," <http://www.soi.wide.ad.jp/class/20070026/slides/04/27.html>, Last Accessed 17.12.2018, 1950.
- A. J. Sørensen, *Marine Cybernetics Towards Autonomous Marine Operations and Systems*, 2018.
- W. Caharija, M. Candeloro, K. Y. Pettersen, and A. J. Sørensen, "Relative velocity control and integral los for path following of underactuated surface vessels," *Relative Velocity Control and Integral LOS for Path Following of Underactuated Surface Vessels*, 2012.
- E. Børhaug, "Nonlinear control and synchronization of mechanical systems," Ph.D. dissertation, Norwegian University of Science and Technology, Trondheim, Norway, 2008.
- Hemisphere, "Vector vs330 gnss compass," <https://hemispheregnss.com/Products/Products/Position-Heading/vector-vs330e284a2-gnss-compass-94>, Last Accessed 14.12.2018, 2018.
- XSENS, "Xsens mti 10-series imu," <https://www.xsens.com/products/mti-10-series/>, Last Accessed 14.12.2018, 2018.
- Torqueedo, "Torqueedo electric pod thruster," <https://www.torqueedo.com/en/products/pod-drives/cruise-2.0-4.0-fp/M-1250-00.html>, Last Accessed 14.12.2018, 2018.

-
- Arduino, "Arduino mega," <https://store.arduino.cc/arduino-mega-2560-rev3>, Last Accessed 14.12.2018, 2018.
- Wachendorff, "Wachendorff absolute encoder," <https://www.wachendorff-automation.com/encoder-absolute-SSI-WDGA36ASSI/>, Last Accessed 14.12.2018, 2018.
- Intecno, "Intecno bldc server motor," <https://www.greenline-intecno.com/wp-content/uploads/2015/05/Manuale-BLDC-XL-03-11-gb.pdf>, Last Accessed 14.12.2018, 2018.
- L. Hoberock, "A survey of longitudinal acceleration comfort studies in ground transportation vehicles," *Department of Transportation office of university research, University of Texas at Austin*, 1976.
- N. Sae-Khow, "Klart for ubemannede skip i trondheimsfjorden," <https://www.nrk.no/trondelag/klart-for-ubemannede-skip-i-trondheimsfjorden-1.13156068>, Last Accessed 17.12.2018, 2016.
- L. Delligatti, *SysML Distilled: A Brief Guide to the Systems Modeling Language*. Pearson Education, 2013.

Appendix A

Media Coverage

During this project, milliAmpère has generated a lot of media attention. The media outlets are an important part of the continued development of autonomous vessels. The media exposure serve as an important part in bringing attention to the field of autonomy and to show the potential of this technology.



Figure A.1: Brage (left) on board milliAmpère during a demo at Sjøsikerkonferansen in Haugesund. Photo courtesy of Teknisk Ukeblad

Articles and media

- NRK TV, milliAmpère på distriktsnyheter (26.09.2018): <https://tv.nrk.no/serie/distriktsnyheter-rogaland/DKRO97092618/26-09-2018#t=2m43s>
- NRK Radio, Innslag i Haugesund (26.09.2018): <https://radio.nrk.no/serie/distriktsprogram-rogaland/DKRO02019318/26-09-2018#t=8m27.16s>
- Skipsrevyen, innslag med milliAmpère (26.09.2018): <https://www.skipsrevyen.no/article/autonomt-innslag-paa-sjoesikkerhetskoneransen/>
- TV Haugaland, visning av milliAmpère (27.09.2018): <https://hnytt.no/2018/09/27/herkjorer-den-forerlose-ferga-i-smedasundet/>
- Teknisk Ukeblad, milliAmpère i Haugesund (28.09.2018): <https://www.tu.no/artikler/her-demonstrerer-de-selvkjorende-milliampere-na-skal-de-bygge-ferge-pa-12-meter/447398?key=aTPPxOqK>
- Stand på DN Havet Konferansen med besøk av kronprins Håkon (16.10.2018): <https://www.facebook.com/havetDN/videos/1130244403799605/>
- Dagens Bilde i Adresseavisa (20.11.2018)

Appendix B

SysML Diagrams

SysML is a great tool for visualizing and breaking down complex systems. SysML is a modelling language and it introduces several concepts to help convey information in a precise and efficient manner. The figures in this appendix are made following the guidelines outlined in (Delligatti, 2013). All figures were created by the author during the course of this project.

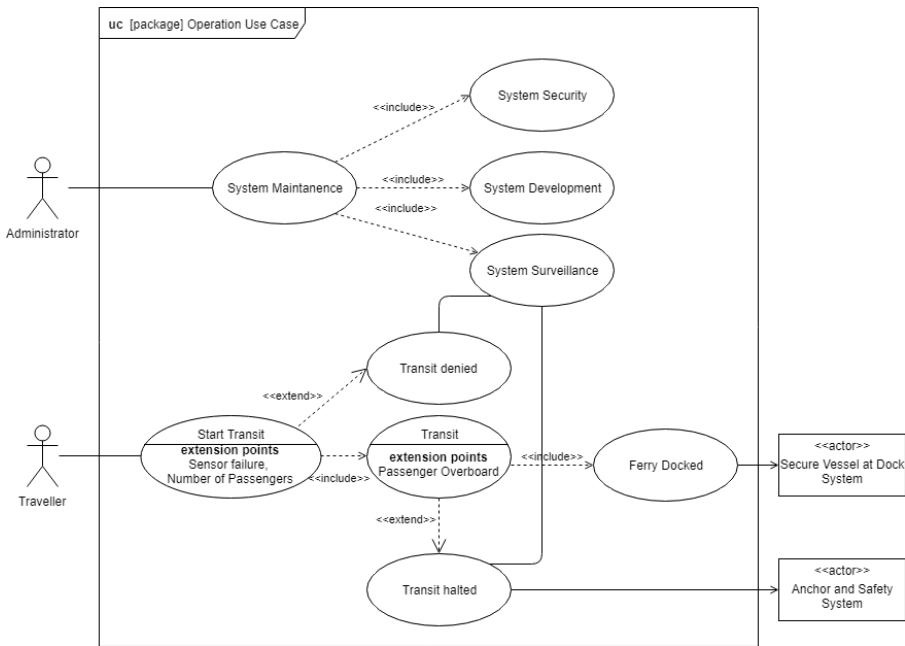


Figure B.1: Use Case Diagram

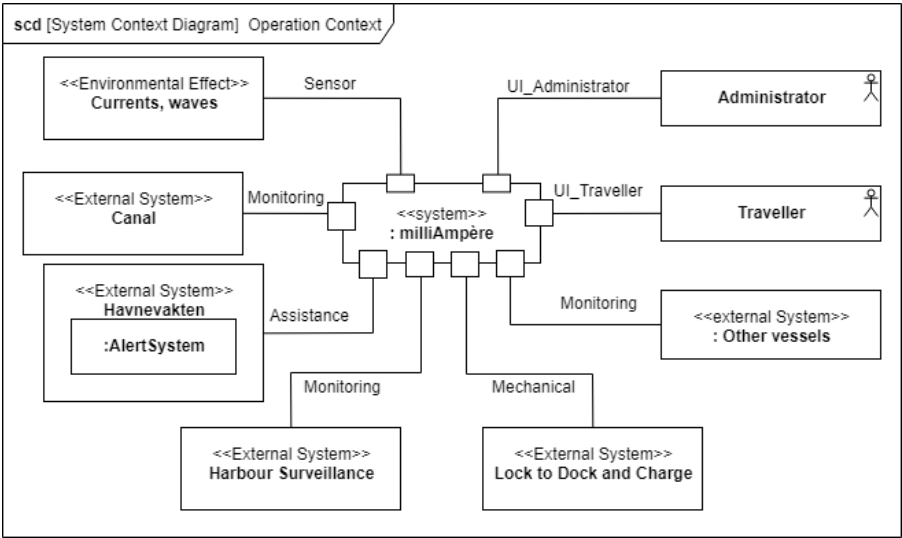


Figure B.2: Context Diagram

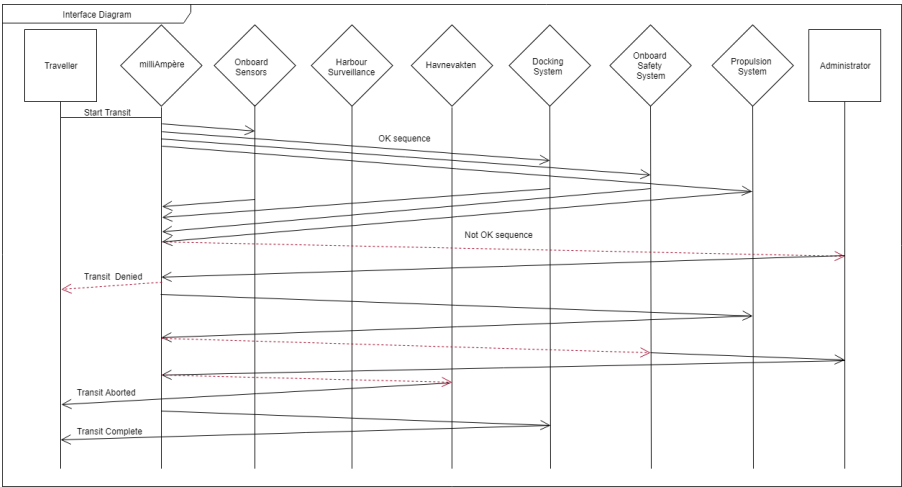


Figure B.3: Interface Diagram

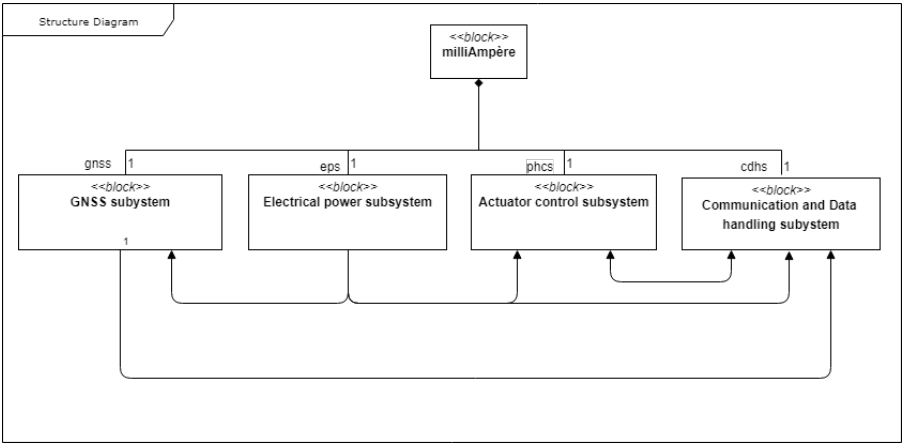


Figure B.4: Structure Diagram

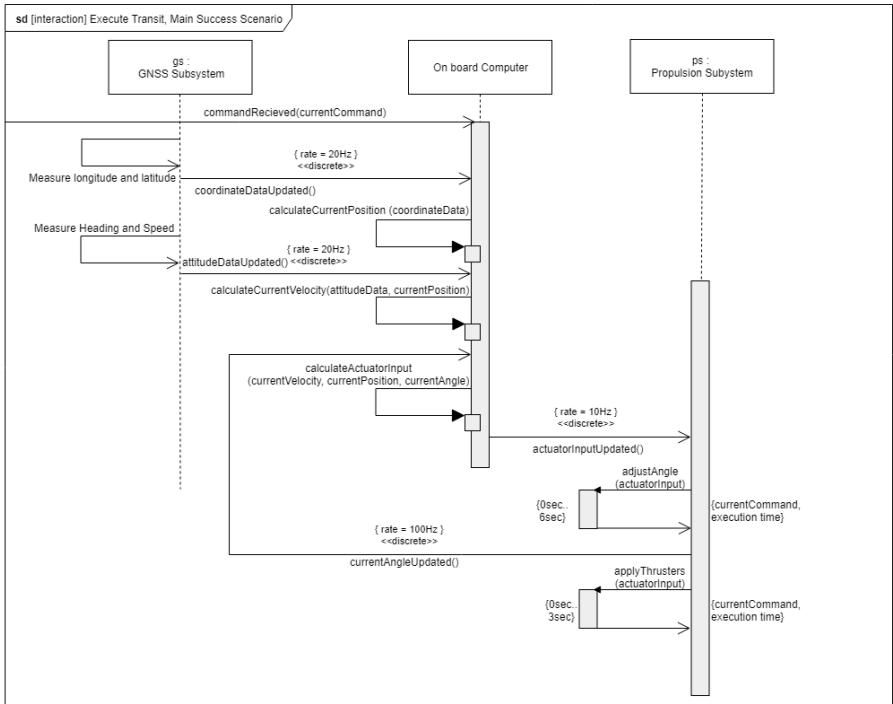


Figure B.5: Sequence Diagram

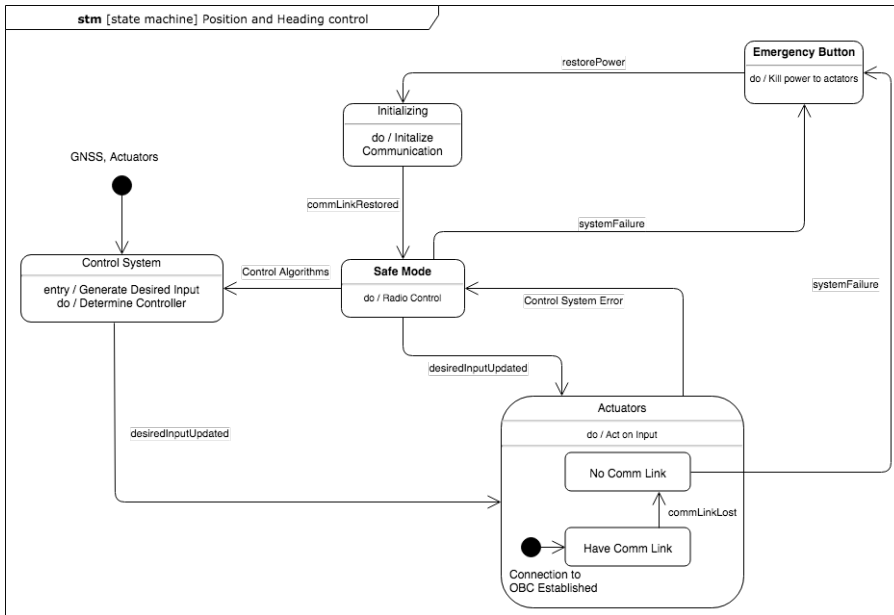


Figure B.6: Control System State Diagram

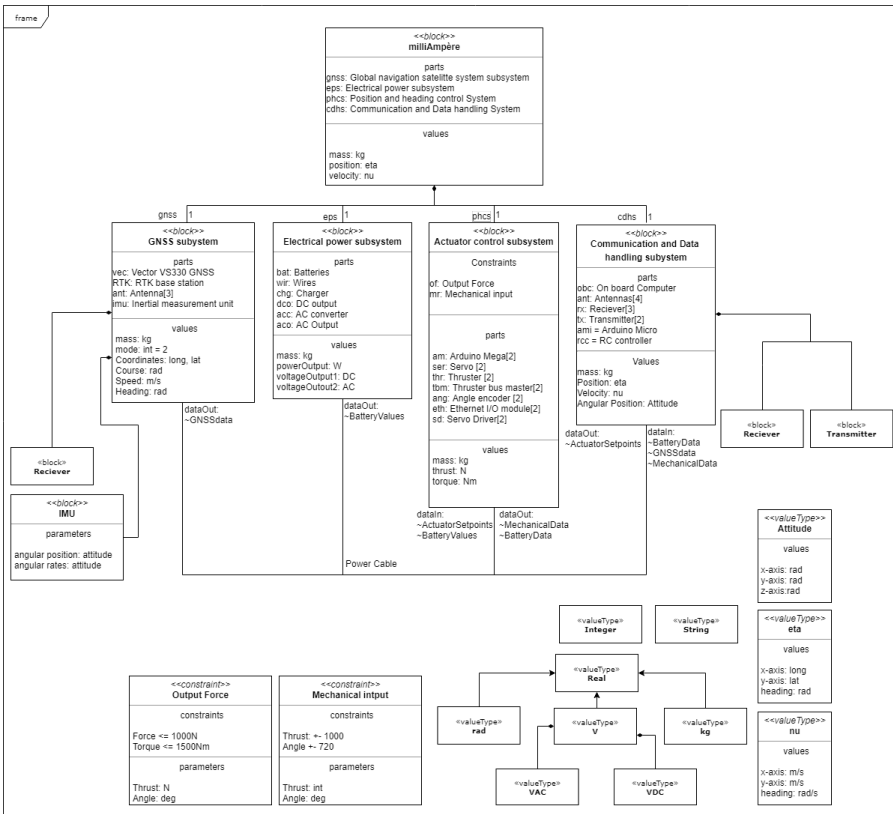


Figure B.7: Class Diagram

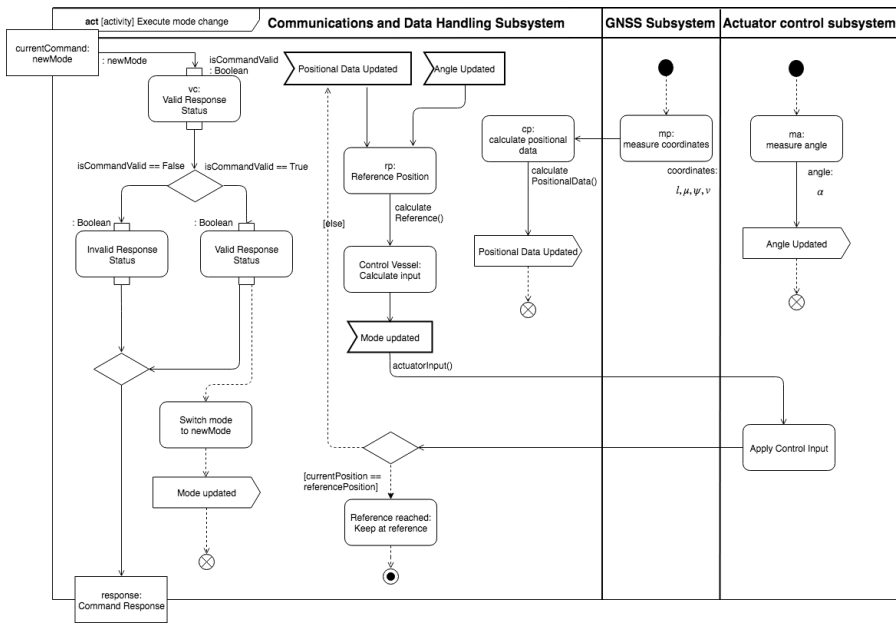


Figure B.8: Mode Change Activity Diagram

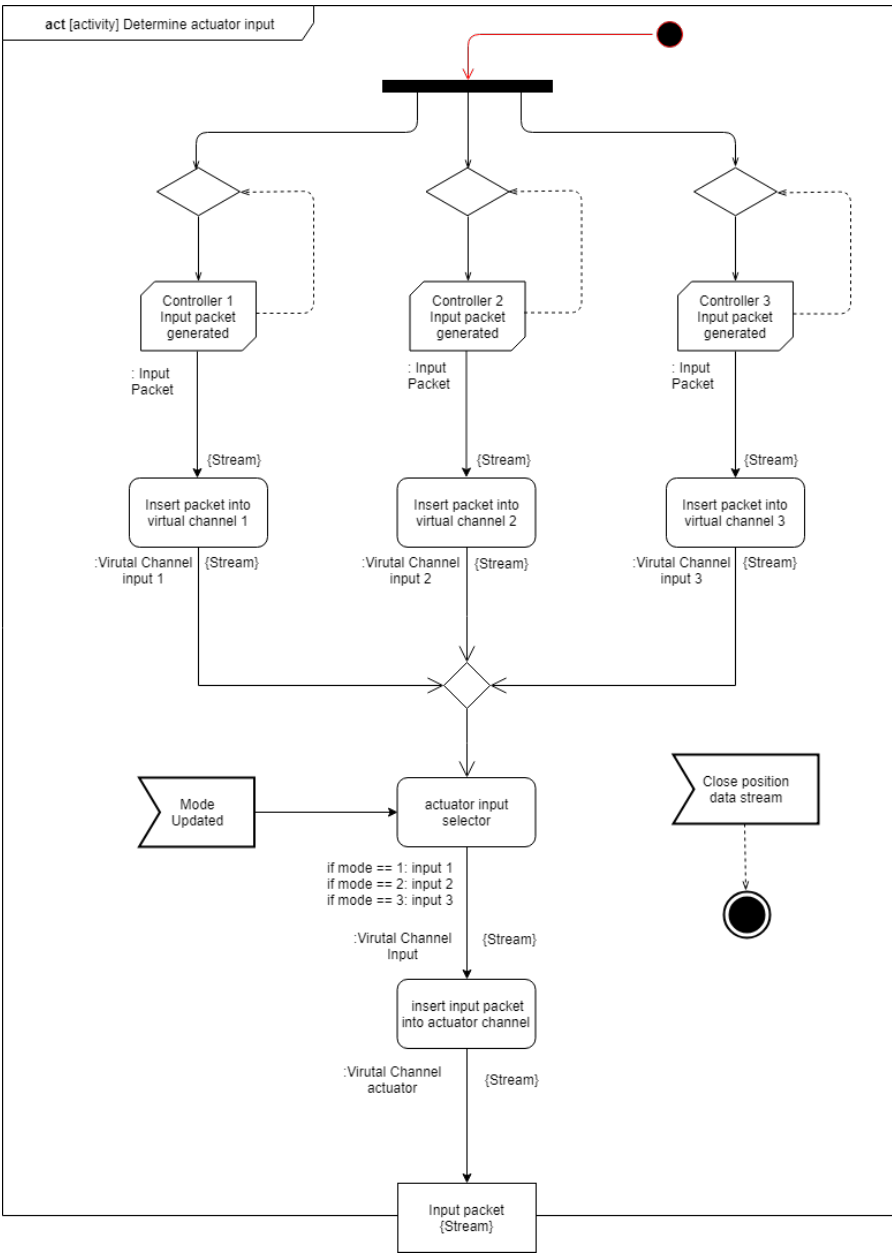


Figure B.9: Determine Input Activity Diagram

Appendix C

GUI

The GUI was made to streamline online testing on milliAmpère. The GUI features interactive buttons providing the possibility of switching states in the state machine. It also visualizes the azimuth thruster angles such that it is easy to discover any potential malfunctions related to the azimuth thrusters. Along with the visualization of the angles of the azimuth thrusters, the GUI presents a lot of data for easier debugging. The GUI has since been updated with a flashing alarm that triggers if any predefined events were to occur.

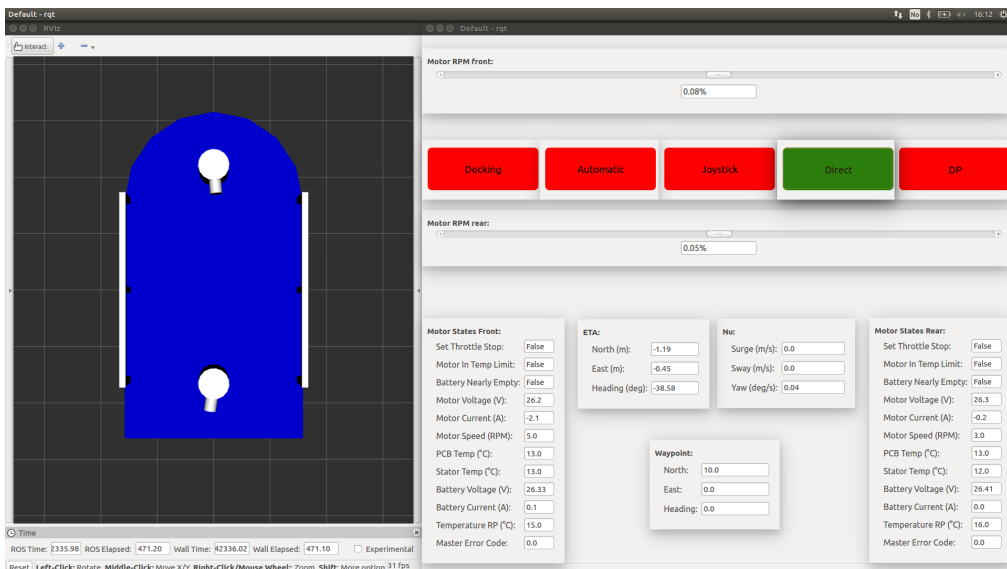
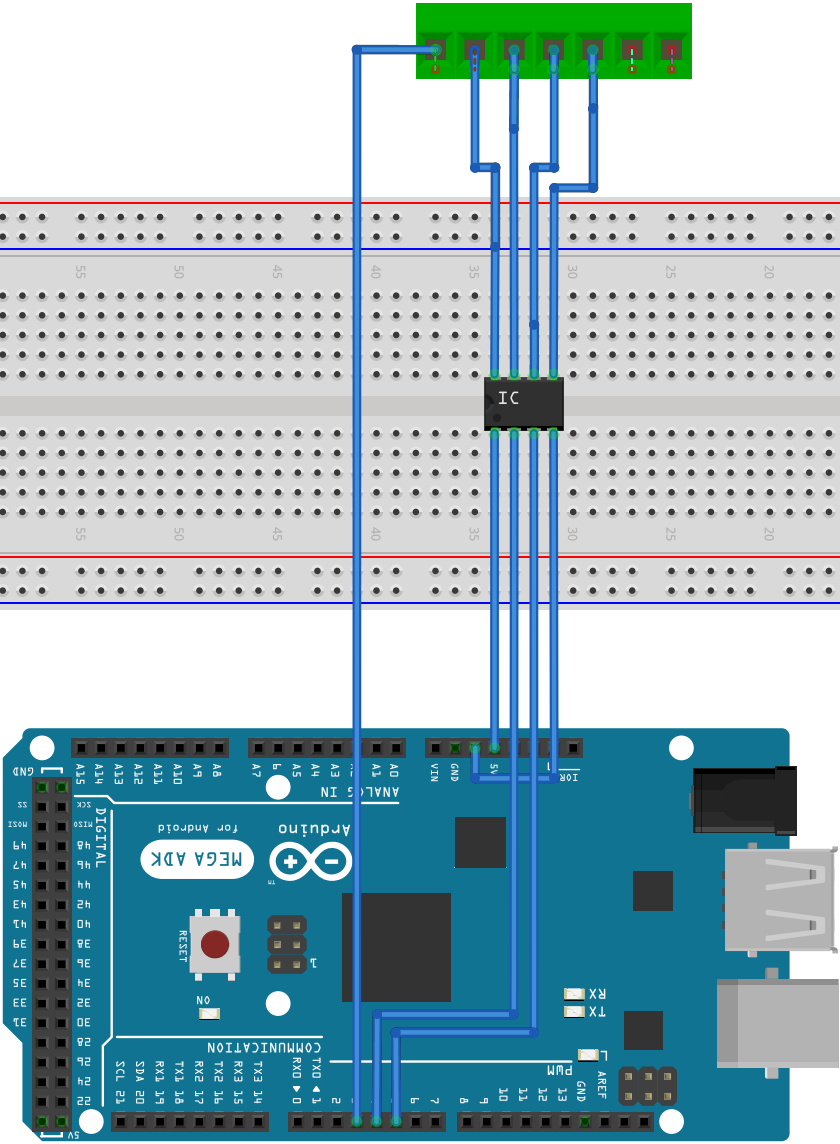


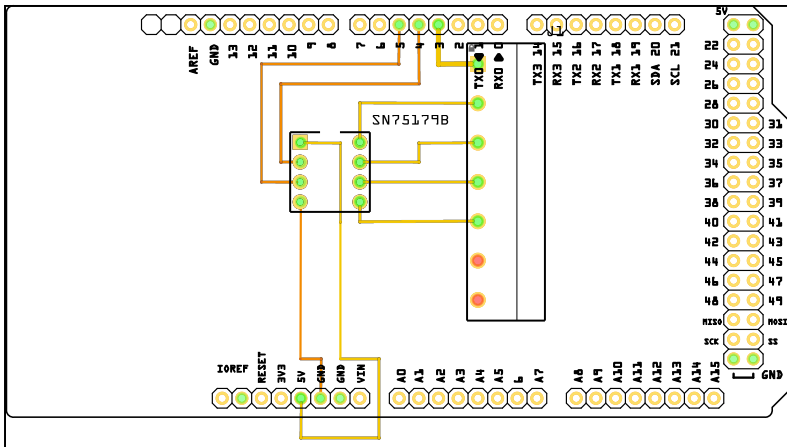
Figure C.1: GUI made with RVIZ, RQT and QT

Appendix **D**

Arduino Shield Specification



Arduino Mega



fritzing

